Supplementary Methods

Mice

SM α-actin-EGFP mice were kindly provided by Dr. Miwa (1). *Aqp2-Cre*, *LysM-Cre* mice were purchased from Jackson Laboratory. UUO was performed as described previously (2). Briefly, the left ureter of anesthetized 10- to 12-week-old mice was ligated at the ureteropelvic junction.

Bone marrow transplantation

Eight-week-old male and female recipient mice were lethally irradiated with a total dose of 11 Gy. The next day unfractionated BM cells (1×10^6) that had been harvested from male donor mice and suspended in 0.22 ml of PBS were administered to each recipient mouse via the tail vein. We confirmed that peripheral leukocytes were reconstituted (>95%) by detecting the Y-chromosome in female mice using in situ hybridization. UUO was then performed in male mice 6 weeks after BM transplantation.

Antibodies

The anti-KLF5 (KM1784, KM3918) antibodies used were described previously (3). Anti-CEBPα (14AA) and anti-AQP2 (H-40) antibodies were from Santa Cruz Biotechnology; anti-Ly-6C, anti Ly-6G, anti-CD11b, anti-F4/80 and anti-CD93 antibodies were from eBioscience; anti-CD31 antibody was from BD; anti-β-galactosidase antibody was from Abcam; anti-CD301 antibody was from GenWay; and anti-CD206 antibody was from AbD Serotec.

Histological analysis

Mice were perfusion-fixed, after which tissues were harvested, further fixed in 10% formalin, dehydrated, embedded in paraffin and sectioned. Tubular injury and interstitial fibrosis were scored by a blind observer in at least 40 cortical fields of PAS-stained samples as described previously (4). For immunohistochemical staining, a Tyramide Signal Amplification kit (Invitrogen) or Envision Plus and a Biotin Blocking System (DakoCytomation) were used. For colorimetric visualization, either DAB (F4/80 and KLF5) or vector red (Ly-6C) was used.

Determination of interstitial fibrosis

To quantitate renal interstitial fibrosis, we stained renal sections with picrosirius red as described previously (5), after which images were captured with a digital camera (Leica) and analyzed for red-staining using Scion Image. Twelve non-overlapping high-power fields (400x magnification) from each section were analyzed by investigators blinded to the protocol.

To analyze areas of interstitium and fibrosis, we employed the point counting method described previously (6). Sections were stained with Azan-Mallory to visualize collagen fibers, and points falling within the interstitial and fibrotic areas were counted. Relative volume was defined as previously described (6). Under high magnification, consecutive non-overlapping fields were photographed from each section of renal cortex. n=6 for each group.

β-Galactosidase staining

Kidneys were fixed for 12 h at 4°C in PBS containing 0.4% glutaraldehyde, 0.01% sodium deoxycholate, 0.1% NP40, 0.1 M $MgCl_2$ and 5 mM EGTA. The fixed tissues were rinsed three times for 30 min each in PBS, and then incubated for 24 h at 37°C in a staining solution (1 mM $MgCl_2$, 20 mM $K_3Fe(CN)_6$, 20 mM $K_4Fe(CN)_6$, 1 mg/ml X-gal in PBS).

Real-time PCR analysis

Total RNA was purified from cells or tissues using RNeasy (Qiagen) according to the manufacturer's instructions. Quantitative real-time PCR analyses were carried out using a Lightcycler system (Roche) with 18s rRNA serving as an internal control. The sequences of the primers used are as follows: *Klf5*, 5'-TGG TTG CAC AAA AGT TTA TAC-3' and 5'-GGC TTG GCG CCC GTG TGC TTC C-3'; *Col1a1*, 5'-AGA CAT GTT CAG CTT TGT GGA C-3' and 5'-GCA GCT GAC TTC AGG GAT G-3'; *Col3a1*, 5'-TCC CCT GGA ATC TGT GAA TC-3' and 5'-TGA GTC GAA TTG GGG AGA AT-3'; *Emr1*, 5'-CCT GGA CGA ATC CTG TGA AG-3' and 5'-GGT GGG ACC ACA GAG AGT TG-3'; *Tnfa*, 5'-ACC CTC ACA CTC AGA TCA TCT TC-3' and 5'- TGG TGG TTT GCT ACG ACG T-3'; *Il1b*, 5'-TTG ACG GAC CCC AAA AGA T -3' and 5'- GAA GCT GGA TGC TCT CAT CTG -3'; *Tgfb1*, 5'-GCA ACA TGT GGA ACT CTA CCA GAA-3' and 5'-GAC GTC AAA AGA CAG CCA CTC A-3'; *Ctgf*, 5'-GTG CCA GAA CGC ACA CTG-3' and 5'-CCC CGG TTA CAC TCC AAA-3'; *Cdh1*, 5'-TGC CCA GAA AAT GAA AAA GG-3' and 5'-AAT GGC AGG AAT TTG CAA TC-3'; *Fn1*, 5'-CTG TGA CAA CTG CCG TAG-3' and 5'-CGA TGC TTG GAG AAG CTG-3'; *Vim*, 5'-GCC TTT TTG AAG AAA CTG CAC GAT G-3' and 5'-CCG GTA CTC GTT TGA CTC

CTG CTT G-3’; *Tlr4*, 5’-GGA CTC TGA TCA TGG CAC TG-3’ and 5’-CTG ATC CAT GCA TTG GTA GGT-3’; *Mrc1*, 5’-GGA CGA GCA GGT GCA GTT-3’ and 5’-CAA CAC ATC CCG CCT TTC-3’; *Ccl3*, 5’-CAA GTC TTC TCA GCG CCA TA -3’ and 5’-GGA ATC TTC CGG CTG TAG G -3’; *Il10*, 5’-TTT GAA TTC CCT GGG TGA GAA-3’ and 5’-ACA GGG GAG AAA TCG ATG ACA-3’; *Ly6c*, 5’-TCT TGT GGC CCT ACT GTG TG -3’ and 5’-GCA ATG CAG AAT CCA TCA GA -3’; *Acta2*, 5’-AGC TGT TTT CCC ATC CAT TG-3’ and 5’-GCG CTT CAT CAC CCA CGT AG-3’; *Cebpa*, 5’-CCT TCA ACG ACG AGT TCC TG-3’ and 5’-TGG CCT TCT CCT GCT GTC-3’; *Cebpb*, 5’-TGA TGC AAT CCG GAT CAA-3’ and 5’-CAC GTG TGT TGC GTC AGT C-3’; *Cebpd*, 5’-GAG AAC GAG AAG CTG CAT CA-3’ and 5’- GGC TGG GCA GTT TTT GAA-3’; *Cebpg*, 5’-ACG AGT TCT GGG CAT AGA GG-3’ and 5’- TGA CCC AAA GGG CTA GAC AG-3’; *Cebpz*, 5’-CGA TGA GGG CAA GAA TGG-3’ and 5’- GCC AGC ATA AGG TAA TCT TGC-3’; *Ccl2*, 5’-CAT CCA CGT GTT GGC TCA-3’ and 5’-GAT CAT CTT GCT GGT GAA TGA GT-3’; *Tlr4*, 5’-GGA CTC TGA TCA TGG CAC TG-3’ and 5’-CTG ATC CAT GCA TTG GTA GGT-3’; *Cd36*, 5’-TTG TAC CTA TAC TGT GGC TAA ATG AGA-3’ and 5’-CTT GTG TTT TGA ACA TTT CTG CTT -3’; *Rage*, 5’-GTG TCG GGC AAC TAA CAG G-3’ and 5’-CTG GCT TCC CAG GAA TCT G -3’; *Cd115* 5’-GAC CAT GGT GAA TGG TAG GG-3’ and 5’- GGA TAA CGT TGA ATC CCA CTG -3’.

Cell culture

mIMCD-3 cells were obtained from the American Type Culture Collection and maintained in Dulbecco’s modified Eagle’s medium/F12 (DMEM/F12, Invitrogen) supplemented with 10%

fetal bovine serum (Hyclone). We used immunocytochemistry to confirm that mIMCD-3 cells expressed AQP2 (data not shown). For plasmid transfection, mIMCD-3 cells were plated to a density of 1.0 x10^4 cells/cm^2 in 12-well culture plates one day prior to transfection. Once the cells reached 50-60% confluence, they were transfected using Polyfect transfection reagent (Qiagen) following the supplier's protocol. Luciferase activities were measured using a luciferase assay system (Promega) and then normalized to the protein concentration in each cell lysate. Primary mouse tubular epithelial cells were cultured as described previously (7). Normal human renal cortical epithelial (HRCE) cells were obtained from Lonza and maintained in BulletKit. Macrophage-conditioned media were prepared by culturing macrophages isolated from kidneys using a FACSAria II cell sorter (BD) in serum-free RPMI 1640 medium for 24 h. Bone marrow-derived macrophages were prepared from wild-type and *Klf5*$^{fl/fl}$;*LysM-Cre* mice as described previously (8).

Collecting duct cell purification

Collecting duct (CD) cells were purified as described previously with minor modifications (9, 10). Briefly, for inner medullary collecting duct (IMCD) cell isolation, renal papillae were excised and placed in ice-cold modified Ringer solution, after which they were minced and incubated with 2 mg/ml collagenase B (Roche Diagnostics) and 600 U/ml hyaluronidase (Worthington) for 50 min, and with 50 U/ml DNase I (Roche Diagnostics) for 20 min. The resultant suspension was subjected to three cycles of centrifugal separation at 50 *g* for 30 s. The cells were then examined under a microscope to determine whether there was

contamination by smaller, non-CD cells. If contaminating non-collecting duct cells were observed in the suspensions, one or two additional centrifugal separations were added. The supernatants were used as non-collecting duct cells, and the cell pellets were used as IMCD cells. To isolate cortical collecting duct (CCD) cells, the remaining kidneys were sliced with a sharp scalpel, placed in ice-cold modified Ringer solution (20 mM Tris/HCl [pH 7.4], 125 mM NaCl, 10 mM KCl, 10 mM sodium acetate, 5 mM glucose), minced, and incubated for 20 min with 2 mg/ml collagenase B (Roche) and 0.2 mg/ml protease type XIV (Sigma Aldrich). CCD segments were identified under a dissection microscope, based on their diameter and specific morphology (11), and isolated. Using a pipette, all of the CCD segments were picked, and the remaining cells were used as non-collecting duct cells. The purity of the CCD cells was analyzed by immunostaining of AQP2 (Supplementary Figure 1B). IMCD and CCD cells were combined and used as CD cells, while cortical and medullary non-CD cells were combined as used as non-CD cells.

Plasmids

The mouse *S100a8* (-330 to +47 bp), *S100a9* (-501 to +400 bp) and *Cebpa* (-509 to +488 bp) promoters and the human *CDH1* (-178 to +66 bp) promoter were cloned from mouse and human genomic DNA by PCR, after which the integrity of the amplified fragments was confirmed by sequencing. The promoter fragments were then cloned into the pGL3 basic vector (Promega). QuickChange site-directed mutagenesis kits were used to generate site directed mutant plasmids (Stratagene).

Flow cytometric analysis

To isolate cells from kidneys, whole kidney was cut into small pieces in ice-cold Paris buffer (20 mM Tris/HCl, 125 mM NaCl, 10 mM KCl, 10 mM sodium acetate, 5 mM glucose) and then collected by centrifugation at 250 *g*. The collected tissue was incubated for 20 min with collagenase type I (1 mg/ml, Sigma Aldrich) and Dnase I (0.1 mg/ml, Sigma Aldrich) in Hanks' buffered saline solution (HBSS). After two washes in HBSS on ice, the tissue was incubated for 20 min with 2 mM EDTA in HBSS and then spun at 30 *g*. The supernatant containing isolated cells was kept on ice. The remaining pellet was subjected to a second enzymatic digestion with 1 mg/ml collagenase I in HBSS for 20 min, after which the suspension was passed three times through a 21-gauge needle and spun at 30 *g*. Cells in the two resultant supernatants were combined, washed twice in HBSS and resuspended in HBSS. After removing any erythrocytes using BD PharmLyse (BD), the samples were subjected to flow cytometric analysis.

Adenovirus-mediated overexpression of KLF5 and microarray analysis

Recombinant adenovirus particles were prepared using a ViraPower Adenoviral Gateway Expression kit (Invitrogen). mIMCD-3 cells were infected with either empty adenovirus (Ad-empty) or human KLF5-expressing adenovirus (Ad-*KLF5*). Forty eight h after infection, total RNA was purified from the cells and subjected to microarray and RT-PCR analyses. Microarray analysis was performed using the GeneChip mouse Expression Set 430

(Affymetrix).

***In vivo* ChIP and re-ChIP assays**

Samples of fresh renal papillary tissue (30 mg) were chopped into small pieces with a razor blade and collected in ice-cold PBS. Formaldehyde was then added to the PBS to a final concentration of 1%, and the samples were incubated at room temperature for 10 min with rotation. The cross-linking reaction was stopped by adding glycine to a final concentration of 0.125 mol/L. After centrifugation at 1200 rpm for 5 min, the resultant pellets were washed three times with ice-cold PBS, and the following ChIP assays were carried out as previously described for cultured cells (12). For sequential ChIP (re-ChIP) assays, cross-linked chromatin samples were immunoprecipitated with either anti-KLF5 or anti-C/EBPα antibody, after which the precipitates were eluted and subjected to another round of ChIP using anti-CEBPα or anti-KLF5 antibody, respectively (13). The sequences of the PCR primers were: *Cebpa* promoter, 5'-GAC TTA GAG GCT TAA AGG AGG GG-3' and 5'-GCG CAA CGC CCA CTG ACT CCT GCG C-3'; *pdgfa* 3' UTR, 5'-GTG ACA TTC CTG AAC ATA CTA TGT ATG GTG-3' and 5'-GTC TCT CCG AGT GCT ACA GTA CTT GCT TTG-3'; *S100a8* proximal promoter, 5'-CAT GAA GGC ATT GGA TCA GCA ATG G-3' and 5'-CAG AGT TGC CAC AGC CTC TGT TTC C-3'; *S100a9* proximal promoter, 5'-AGG AAG GGA AGT GAG CCA ACT A-3' and 5'-GGA AGA TTG CTT CAC AGG TGA GCA G-3'; *Cdh1* promoter, 5'-TTG TAA CTC CAT GTC TCC GTG GGT C-3' and 5'-CGC CAG GTG AGC CCG CAG GCA CCG-3'.

Mammalian two-hybrid assay

The full-length *Klf5* cDNA was fused to the Gal4 DNA binding domain in the vector pBIND (Promega) to generate pBIND-*Klf5*. The full-length *Cebpa* cDNA was fused to the VP16 activation domain in pACT (Promega) to generate pACT-*Cebpa*. We transfected those constructs along with the reporter pSG5 (Promega) into mIMCD-3 cells using PolyFect transfection reagent (Invitrogen).

Coimmunoprecipitation assay

Lysates of mIMCD-3 cells expressing flag-tagged KLF5 and C/EBPα were immunoprecipitated with either anti-flag or anti-C/EBPα antibody (Santa Cruz Biotechnology). The immunoprecipitates were then probed for C/EBPα or KLF5.

Analysis of RAW264.7 cell and bone marrow-derived macrophage migration

mIMCD-3 cells were cultured in the bottom wells of a 24-well multiwell Boyden chamber system (Becton Dickinson) in DMEM/F12 supplemented with 10% FBS. Once the cells reached 60-70% confluence, they were infected with 5 MOI of KLF5-expressing adenovirus. Twelve hours after addition of adenovirus, the cells were washed three times with PBS and cultured for an additional 24 h in DMEM/F12 supplemented with 3% FBS. For transfection of siRNA, the medium was replaced with serum-free Opti-MEM 12 h after addition of the adenovirus, and siRNA was transfected using Lipofectamine 2000 (Invitrogen). After

transfection, the cells were washed three times with PBS and cultured for additional 24 h in DMEM/F12 supplemented with 3% FBS. RAW264.7 cells and bone marrow-derived macrophages stained with Calcein-AM (Dojindo Molecular Technologies) were plated on Fluoroblok cell culture inserts with 3.0 μm pores (Becton Dickinson), and the migrated cells were analyzed by fluorescent microscopy.

Small interfering RNA (siRNA)

An siRNA mixture for *Klf5* (ON-TARGET plus SMART pool) and the control ON-TARGETplus siCONTROL were purchased from Dharmacon. siRNAs for *S100a8* and *S100a9* were generated using a silencer siRNA construction kit (Ambion) according to the manufacturer's instructions. The sequences targeted by the siRNAs were: 5'-GAA AGA GAA GAG AAA TGA A -3' (*S100a8*) and 5'-GTT TGA AAG GAA ATC TTT C-3' (*S100a9*). A scrambled nucleotide sequence for each siRNA was used as a control. mIMCD-3 cells cultured in 6-cm dishes were transfected with 280 ng of siRNA using a Deliver X kit (Genospectra) according to the manufacturer's instructions.

Apoptosis analysis

To detect apoptotic cells in tissues, paraffin embedded kidneys were processed for TUNEL staining using ApopTag In Situ Apoptosis Detection Kit (Millipore) as described previously (14). For TUNEL staining of cultured cells, an in situ cell death detection kit POD (Roche) was used according to the manufacture's instruction. $TUNEL^+$ cells that exhibited at least one of the

following features were considered to be apoptotic: nuclear chromatin marginalization and fragmentation, nuclear and cellular condensation and blebbing, and the presence of membrane-bound apoptotic bodies with preserved organelles and occasional nuclear fragments (14). For annexin V apoptosis assays, cells isolated from kidneys were stained with annexin V and FITC using an Annexin V-FITC apoptosis detection kit (Beckman Coulter) according to the manufacture's instructions and then analyzed by flow cytometry.

Cre-mediated recombination

The deletion frequency was determined by PCR amplification using the primers 5'-GTCTCGGCCTCATTGCTAAG-3' and 5'-TGACCCATTACCGAATCTACTG-3', which produce 331-bp and 250-bp bands for the floxed and floxed-out *Klf5* alleles, respectively (15).

Urine creatinine concentration analysis

Twenty-four hour urine samples were analyzed using ELISA kits (Exocell).

Adoptive transfer of bone marrow cells

Bone marrow cells were harvested from the femurs and tibias of *CAG-EGFP* transgenic mice (Japan SLC). Red blood cells were depleted using Phamlyse (BD), after which the $GFP^+CD11b^+Ly\text{-}6C^+$ cells were isolated using FACSAria II (BD). The collected cells were then washed, resuspended in PBS and intravenously injected into wild-type recipient mice ($1x10^6$ cells/mouse), as described previously (16). UUO and S100A8/S100A9 injections were

carried out immediately after the adoptive transfer. For flow cytometric analyses, circulating cells were collected 12 h after the adoptive transfer, and kidney cells were isolated 24 h after UUO or S100A8/A9 injection.

Bone marrow-derived macrophage (BMDM) culture and M1, M2 activation

Bone marrow-derived macrophages were cultured as described previously from adult wild-type, *Klf5*$^{+/-}$, and *Klf5*$^{fl/fl}$*;LysM-Cre* mice (17). Briefly, BM cells were obtained from bilateral femurs and tibias and transferred to RPMI1640 supplemented with 10% FBS. Red blood cells were lysed in lysis buffer (Pharmlyse, BD). Cells were washed once in medium and then plated and cultured for 7 days in RPMI1640 supplemented with 1% penicillin/streptomycin, 1% HEPES, 0.001% mercaptoethanol, 10% FBS and 30 ng/ml M-CSF (macrophage colony stimulating factor) (18). To promote differentiation into M1 or M2 macrophages, cells were treated for 12-24 h with LPS (100 ng/ml; Sigma-Aldrich) plus IFNγ (20 ng/ml; BD) or IL-4 (20 ng/ml; BD), respectively (19).

Interleukin 1 receptor antagonist administration

Following UUO, 1 mg/kg interleukin 1 receptor antagonist (IL-1RA, anakinra) or PBS (vehicle) was intraperitoneally administrated to mice daily (20).

Quantitative Western Blotting

For quantitative analysis, Western blots were captured using an Odyssey infrared imaging

system (Licor) and analyzed using ImageStudio (Licor). Band intensity was normalized to that of β-Tubulin.

Statistical analyses

Comparisons between two groups were made using Student's *t* test. Differences among more than two groups were analyzed using one-way ANOVA followed by Bonferroni (3 groups) or Tukey-Kramer post-hoc (>4 groups) tests. Values of $P<0.05$ were considered significant. Error bars represent the S.D. except where otherwise indicated.

Supplementary References

1. Nakano Y, Nishihara T, Sasayama S, Miwa T, Kamada S, Kakunaga T. Transcriptional regulatory elements in the 5' upstream and first intron regions of the human smooth muscle (aortic type) alpha-actin-encoding gene. *Gene*. 1991;99(2):285-289.
2. Ophascharoensuk V, et al. Obstructive uropathy in the mouse: Role of osteopontin in interstitial fibrosis and apoptosis. *Kidney Int*. 1999;56(2):571-580.
3. Oishi Y, et al. SUMOylation of Kruppel-like transcription factor 5 acts as a molecular switch in transcriptional programs of lipid metabolism involving PPAR-delta. *Nat Med*. 2008;14(6):656-666.
4. Pichler RH, et al. Pathogenesis of cyclosporine nephropathy: roles of angiotensin II and osteopontin. *J Am Soc Nephrol*. 1995;6(4):1186-1196.
5. Duffield JS, et al. Conditional ablation of macrophages halts progression of crescentic glomerulonephritis. *Am J Pathol*. 2005;167(5):1207-1219.
6. Ishidoya S, Morrissey J, McCracken R, Reyes A, Klahr S. Angiotensin II receptor antagonist ameliorates renal tubulointerstitial fibrosis caused by unilateral ureteral obstruction. *Kidney Int*. 1995;47(5):1285-1294.
7. Breggia AC, Himmelfarb J. Primary mouse renal tubular epithelial cells have variable injury tolerance to ischemic and chemical mediators of oxidative stress. *Oxid Med Cell Longev*. 2008;1(1):33-38.
8. Erwig L-P, Kluth DC, Walsh GM, Rees AJ. Initial cytokine exposure determines function of macrophages and renders them unresponsive to other cytokines. *J Immunol*.

1998;161(4):1983-1988.

9. Chou CL, DiGiovanni SR, Luther A, Lolait SJ, Knepper MA. Oxytocin as an antidiuretic hormone. II. Role of V2 vasopressin receptor. *Am J Physiol*. 1995;269(1 Pt 2):F78-85.

10. Schlatter E, Frobe U, Greger R. Ion conductances of isolated cortical collecting duct cells. *Pflugers Arch*. 1992;421(4):381-387.

11. Schafer JA, Watkins ML, Li L, Herter P, Haxelmans S, Schlatter E. A simplified method for isolation of large numbers of defined nephron segments. *Am J Physiol*. 1997;273(4):F650-F657.

12. Fujiu K, et al. Synthetic retinoid Am80 suppresses smooth muscle phenotypic modulation and in-stent neointima formation by inhibiting KLF5. *Circ Res*. 2005;97(11):1132-1141.

13. Metivier R, et al. Estrogen receptor-alpha directs ordered, cyclical, and combinatorial recruitment of cofactors on a natural target promoter. *Cell*. 2003;115(6):751-763.

14. Hughes J, Gobe G. Identification and quantification of apoptosis in the kidney using morphology, biochemical and molecular markers. *Nephrology*. 2007;12(5):452-458.

15. Takeda N, et al. Cardiac fibroblasts are essential for the adaptive response of the murine heart to pressure overload. *J Clin Invest*. 2010;120(1):254-265.

16. Lin SL, Castano AP, Nowlin BT, Lupher ML, Jr., Duffield JS. Bone marrow Ly6Chigh monocytes are selectively recruited to injured kidney and differentiate into functionally distinct populations. *J Immunol*. 2009;183(10):6733-6743.

17. Longbrake EE, Lai W, Ankeny DP, Popovich PG. Characterization and modeling of monocyte-derived macrophages after spinal cord injury. *J Neurochem*. 2007;102(4):1083-1094.

18. Burgess AW, et al. Purification of two forms of colony-stimulating factor from mouse L-cell-conditioned medium. *J Biol Chem*. 1985;260(29):16004-16011.

19. Liu Y, et al. Unique expression of suppressor of cytokine signaling 3 is essential for classical macrophage activation in rodents in vitro and in vivo. *J Immunol*. 2008;180(9):6270-6278.

20. Abbate A, et al. Anakinra, a Recombinant Human Interleukin-1 Receptor Antagonist, Inhibits Apoptosis in Experimental Acute Myocardial Infarction. *Circulation*. 2008;117(20):2670-2683.

21. Iwata H, et al. Bone marrow-derived cells contribute to vascular inflammation but do not differentiate into smooth muscle cell lineages. *Circulation*. 2010;122(20):2048-2057.

22. Vermes I, Haanen C, Steffens-Nakken H, Reutellingsperger C. A novel assay for apoptosis Flow cytometric detection of phosphatidylserine expression on early apoptotic cells using fluorescein labelled Annexin V. *J Immunol Methods*. 1995;184(1):39-51.

Supplementary Figure Legends

Supplementary Figure 1. Collecting duct-specific KLF5 expression

(A) KLF5 expression was confined to AQP-2-expressing cells in the cortical and medullary collecting ducts. KLF5 (red), AQP-2 (green) and nuclei (blue) are shown. Scale bar, 10 μm. (B) Efficacy of the isolation of collecting duct (CD) epithelial cells from kidney. Isolated CD cells and non-CD cells were collected using Cytospin and immunostained with either anti-AQP2 antibody or normal IgG. Scale bar, 20μm. The graph shows the $AQP2^+$ CD cell fractions in each preparation. $^*P<0.05$. n=3. (C) *Klf5*, *Cebpa*, *S100a8* and *S100a9* expression in various cell types in UUO kidneys. *Klf5* mRNA expression was analyzed in cells prepared from UUO kidneys at the indicated times. Collecting duct (CD) cells were isolated using a centrifugal method. $CD11b^+F4/80^+$ and $CD31^+$ (endothelial cells) cells were FACS-sorted from wild-type mice subjected to UUO. SM α-$actin^+$ (myofibroblasts and smooth muscle cells) cells were FACS-sorted from SM α-actin-*EGFP* mice (21) subjected to UUO. Cardiac fibroblasts were isolated from wild-type mice (15). Data labeled day 0 show gene expression in kidneys under basal conditions. Expression levels were normalized first to those of 18s rRNA and then further normalized to the levels in kidneys from control mice. n=3. $^\#P<0.05$ vs. the same cell type at day 0.

Supplementary Figure 2. UUO-induced renal injury is reduced in *Klf5*$^{+/-}$ kidneys

(A) Representative hematoxylin and eosin-stained sections of renal papilla from wild-type and *Klf5*$^{+/-}$ kidneys showing the collecting ducts under basal conditions. Scale bars, 50 μm. (B)

Hematoxylin and eosin and Periodic acid-Schiff (PAS) staining of kidney sections 7 days after UUO. Scale bars, 20 μm. (C) Renal weight/body weight ratios, tubular injury score and interstitial fibrosis score for wild-type and *Klf5*$^{+/-}$ mice after sham operation or UUO. Note that the pelvises were removed before making kidney weight measurements. $^{\#}P<0.05$ vs. WT at the same time point. n=6 for each point.

Supplementary Figure 3. Effects of *Klf5* haploinsufficiency on apoptosis and fibrosis

(A) Representative TUNEL staining of renal cortex and medulla sections from wild-type and *Klf5*$^{+/-}$ mice 4 days after UUO and from sham-operated wild-type mice. Quantification of TUNEL^{+} cells is shown in Figure 1H. Brown, TUNEL^{+} cells; blue, nuclei. Scale bars, 50 μm. (B) Flow cytometric analysis of apoptotic and necrotic cells in kidneys from wild-type and *Klf5*$^{+/-}$ mice 1 day after sham operation or UUO. Annexin V and PI staining of total kidney cells are shown. AnnexinV^{+}PI^{-} cells are early apoptotic cells and AnnexinV^{+}PI^{+} cells are late apoptotic and necrotic cells (22). $^{*}P<0.05$ vs. the sham-operated group for the same genotype. $^{\#}P<0.05$. n=5-6 for each group. (C) Representative picrosirius red staining 14 days after UUO. Quantification of picrosirius red-positive areas is shown in Figure 1H. Scale bar, 50 μm. (D) Relative volumes of the interstitial and fibrotic areas within the kidney cortex 14 days after UUO were determined using the point counting method (6). Relative fibrotic areas within the interstitial area are also shown. n=6 for each group. $^{*}P<0.05$ vs. wild-type.

Supplemental Figure 4. Characterization of macrophages accumulating in the kidney in response to UUO

(A) Forward scatter (FSC)/side scatter (SSC) plots of cells isolated from wild-type kidneys subjected to UUO. We set a gate (R3) for the cell population increased by UUO. Because a majority of $CD11b^+$ cells were located within R3, we analyzed cells gated to R3. (B) Surface expression of M1 and M2 markers in $CD11b^+F4/80^{low}$ (R1) and $CD11b^+F4/80^{hi}$ cells on days 1 and 7 after UUO. (C) FSC and SSC of $CD11b^+F4/80^{low}$ and $CD11b^+F4/80^{hi}$ cells at the indicated times after UUO. (D) Giemsa-stained Cytospin preparations of sorted $CD11b^+F4/80^{low}$ and $CD11b^+F4/80^{hi}$ cells at the indicated times after UUO. (E) Surface F4/80 and CD11b levels on circulating $CD11b^+Ly\text{-}6C^+$ inflammatory monocytes and $CD11b^+F4/80^{low}$ cells on day 1 after UUO. Shown are representative plots.

Supplementary Figure 5. $CD11b^+F4/80^+$, $F4/80^+$, and $Ly\text{-}6C^+$ cells in UUO kidneys

(A, B) $CD11b^+F4/80^{low}$ and $CD11b^+F4/80^{hi}$ cells expressed as fractions among the total kidney cells (A) and the numbers per kidney (B) isolated from the kidneys of wild-type and $Klf5^{+/-}$ mice subjected to UUO. Note that the same data expressed as fractions among living cells are shown in Figure 4B. $^*P<0.05$ vs. mice of the same genotype on day 0. $^{\#}P<0.05$ vs. wild-type at the same time point. n=6 for each group. (C, D) Representative images of F4/80 (C) and Ly-6C (D) staining in kidneys from WT and $Klf5^{+/-}$ mice one day after UUO. The $F4/80^+$ and $Ly\text{-}6C^+$ cell fractions are shown. For quantitation of the $Ly\text{-}6C^+$ cell fractions, endothelial cells, which are also positive for Ly-6C, were excluded. n=5 mice in each group. For

quantification of positively stained cells, at least 12 sections from each region were analyzed. $^{\#}P<0.05$ vs. wild-type. Scale bars, 100μm.

Supplementary Figure 6. Expression of dendritic cell markers in splenic and renal cells

Expression of surface dendritic cell (DC) markers was analyzed in freshly isolated splenic classical $CD11c^{hi}$ DCs (A) and renal $CD11b^{+}F4/80^{hi}$ (B) and $CD11b^{+}F4/80^{low}$ (C) cells. Shown are representative plots. (D) $CD11c^{hi}$ cells identified among $CD45^{+}$ cells were further analyzed for their surface phenotypes. Black and red lines indicate isotype-matched negative controls and specific staining, respectively.

Supplementary Figure 7. Renal $CD11c^{hi}$ cells

(A, B) Giemsa-stained Cypospin preparations of sorted splenic classical DCs (A) and renal $CD11c^{hi}$ cells (B). (C) FSC and SSC plots of renal $CD11c^{hi}MHCII^{+}CD83^{+}$ cells. The R3 gate (Supplementary Figure 4) used to identify $CD11b^{+}$ cells is indicated. (D) $CD11c^{hi}MHCII^{+}CD83^{+}$ cell fractions among the total live cells in UUO kidneys. n=3 for each group.

Supplementary Figure 8. Purity of sorted cells and characterization of renal $CD11b^{+}F4/80^{low}$ and $CD11b^{+}F4/80^{hi}$ cells in culture

(A) Sorted $CD11b^{+}F4/80^{low}$ and $CD11b^{+}F4/80^{hi}$ cells were further analyzed by flow cytometry for CD11b and F4/80 levels, and the purity of the sorted $CD11b^{+}F4/80^{+}$ cells is shown. n=3 for each group. (B, C) $CD11b^{+}F4/80^{low}$ and $CD11b^{+}F4/80^{hi}$ cells were isolated from kidneys

and cultured in serum-free RPMI 1640 medium for 24 h to prepare conditioned medium as in Figure 5. (B) The surface phenotypes of cells cultured for 24 h were analyzed by flow cytometry. (C) Cytokine gene expression was analyzed in the cultured cells. Expression levels were analyzed using real-time PCR, normalized to those of 18s rRNA and then further normalized to those in either $CD11b^{+}F4/80^{hi}$ (*Il1b* and *Ccl2*) or $CD11b^{+}F4/80^{low}$ (*Il10* and *Tgfb1*) cells. n=3 for each group. $^{*}P<0.05$.

Supplementary Figure 9. Effects of IL1-RA on UUO-induced renal injury

Wild-type mice were administered with PBS (vehicle) or IL-1RA, as shown in Figure 2E**,** and renal pathology at the indicated times was analyzed. $^{\#}P<0.05$ vs. PBS-administered mice at the same time point. n=6 for each group.

Supplementary Figure 10. Effects of conditioned media and S100A8/A9 on bone marrow-derived macrophages (BMDMs)

(A) Activation of BMDM migration by mIMCD-3 cells overexpressing KLF5. BMDMs were treated with either IFN-γ and LPS or IL-4 to induce M1 and M2 activation, respectively. The M1- and M2-activated BMDMs were then plated in the inserts of Boyden chambers. The mIMCD-3 cells were infected with empty adenovirus (Ad-empty), adenovirus expressing β-galactosidase (Ad-*LacZ*) or adenovirus expressing KLF5 (Ad-*KLF5*), as indicated, and plated in the bottom wells of the chambers. The numbers of BMDMs that migrated through the porous membranes per high-power field (HPF) during the 8-h incubation period are shown.

n=12. *P<0.05. (B) Effects of recombinant S100A8 and S100A9 on M1- and M2-activated BMDM migration. Recombinant S100A8 and/or S100A9 were added to the medium in the lower wells, as shown. n=6. *P<0.05 vs. the same cell-type without S100 proteins. $^{\#}P$<0.05 vs. M1-activated BMDMs under the same conditions. (C) Knockdown of *S100a8* and *S100a9* in mIMCD-3 cells overexpressing KLF5. Real-time PCR analysis of *S100a8* and *S100a9* expression in KLF5-overexpressing mIMCD-3 cells transfected with siRNAs, as shown in Figure 6E. n=6. *P<0.05 vs. control siRNA. (D) Effects of *S100a8* and/or *S100a9* knockdown in mIMCD-3 cells overexpressing KLF5 on BMDM migration. mIMCD-3 cells overexpressing KLF5 were transfected with siRNAs against *S100a8* and *S100a9* or control siRNA (siCtrl), as indicated, after which they were plated in the bottom wells of Boyden chambers, as shown. The numbers of BMDMs that migrated during the 8-h incubation period are shown. n=6. *P<0.05. $^{\#}P$<0.05 vs. M1-activated BMDMs under the same conditions.

Supplementary Figure 11. Pathological effects of S100A8 and S100A9 on kidneys

Pathological effects of S100A8/A9 injection into kidneys of wild-type mice. Mice were randomly assigned to two groups: one group received three renal injections of S100A8/A9 (days 0, 2 and 4; 25 μg each), while the other group was injected with PBS. Shown are renal injury scores at the indicated times. Bars on day 0 show levels in mice sacrificed soon after the sham operation. *P<0.05 vs. the control (day 0) for the same treatment. $^{\#}P$<0.05 vs. mice injected with PBS at the same time point. n=6 for each group.

Supplementary Figure 12. Adoptive transfer of bone marrow CD11b$^+$Ly-6C$^+$ inflammatory monocytes

(A, B) EGFP$^+$CD11b$^+$Ly-6C$^+$ bone marrow (BM) cells were prepared from *CAG-EGFP* mice and adoptively transferred to wild-type mice just prior to sham operation or UUO ($1x10^6$ cells/mouse). Twenty-four hours after UUO, the transferred EGFP$^+$ cells recruited to the kidneys were analyzed by flow cytometry. In B, mRNA expression levels were analyzed in isolated EGFP$^+$CD11b$^+$Ly-6C$^+$ BM cells, EGFP$^+$CD11b$^+$Ly-6C$^+$ cells in circulation 12 h after adoptive transfer, and kidney EGFP$^+$CD11b$^+$F4/80$^+$ cells 1 and 3 days after UUO. Expression levels were normalized first to those of 18s rRNA and then further normalized to the level in BM EGFP$^+$CD11b$^+$Ly-6C$^+$ cells. **P*<0.05 vs. BM EGFP$^+$CD11b$^+$Ly-6C$^+$ cells. n=3. (C) EGFP$^+$CD11b$^+$Ly-6C$^+$ BM cells were adoptively transferred to wild-type mice prior to renal injection of S100A8/A9 (25 μg of each), as shown in Figure 8C. mRNA expression levels in adoptively transferred cells were analyzed as B. **P*<0.05 vs. BM EGFP$^+$CD11b$^+$Ly-6C$^+$ cells. n=3.

Supplementary Figure 13. Effects of injection of S100A8/A9 into *Klf5*$^{+/-}$ kidneys

S100A8/A9 (25 μg each) were injected into the kidneys of wild-type and *Klf5*$^{+/-}$ mice three times (days 0, 2 and 4) after UUO. (A) Kidney CD11b$^+$F4/80$^+$ cells were analyzed by flow cytometry at indicated times after UUO. $^{\#}$*P*<0.05 vs. the wild-type PBS group at the same time point. **P*<0.05. n=3 for each group. Data on day 0 indicate cells in the kidneys of mice that were sacrificed soon after the sham operation. (B) Renal pathology of the mice at

the indicated times after UUO. $^{\#}P<0.05$ vs. the wild-type PBS group at the same time point. $*P<0.05$. Data on day 0 indicate cells in kidneys of mice that were sacrificed soon after the sham operation. n=3.

Supplemental Figure 14. KLF5 controls *Cebpa* expression

(A) Effects of KLF5 overexpression on expression of members of the C/EBP transcription factor family in mIMCD-3 cells. Expression levels were analyzed by real-time PCR and normalized to those of 18s rRNA. Shown are fold increases in expression in mIMCD-3 cells infected with KLF5-expressing adenovirus, as compared to cells infected with empty adenovirus. n=3. (B) Effects of *Klf5* knockdown on *Cebpa* expression in mIMCD-3 cells. Expression levels were analyzed using real-time PCR, normalized to those of 18s rRNA and then further normalized those in cells transfected with control siRNA (siCtrl). n=3. (C) Western blot showing expression of KLF5 and C/EBPα in cells transfected with either control siRNA (siCtrl) or siRNA targeting *Klf5* (si*Klf5*).

Supplemental Figure 15. ChIP analysis and KLF5-dependent activation of the *Cdh1* expression

(A) ChIP assays for KLF5 (left panel) and C/EBPα (right panel) binding to a nontarget region (*Pdgfa* 3'UTR) in renal papillary cells isolated from kidneys subjected to either UUO or sham operation. One percent of the input chromatin from papillary cells isolated from sham-operated kidneys was used as a positive control (Input). (B) Sequential *in vivo* ChIP (re-ChIP) analysis of the simultaneous binding of KLF5 and C/EBPα to a nontarget region.

Chromatin samples prepared from renal papillary cells were subjected to immunoprecipitation using KLF5 or C/EBPα antibody. The immunoprecipitates were then pulled down further using C/EBP α or KLF5 antibody, respectively. The amount of immunoprecipitated *Pdgfa* 3'UTR region was quantified by PCR. (C) *Cdh1* expression in kidneys under basal conditions. Levels of *Klf5* and *Cdh1* expression were analyzed using real-time PCR. Expression levels were normalized first to those of 18s rRNA and then further normalized to the levels in the kidneys from WT mice. **P*<0.05. n=3 for each group. (D) *Klf5* expression was knocked down using siRNA in mIMCD-3 cells. Levels of *Klf5* and *Cdh1* expression were analyzed using real-time PCR. Expression levels were normalized first to those of 18s rRNA and then further normalized to the levels in the cells transfected with controls siRNA. **P*<0.05. n=6. (E) Effects of KLF5 on *CDH1* promoter activity. mIMCD-3 cells were cotransfected with a *CDH1* promoter reporter plasmid and either CAG-empty or CAG-*KLF5*, as indicated. **P*<0.05. n=6.

Supplementary Figure 16. Effects of bone marrow-specific *Klf5* haploinsufficiency on the response to UUO

Wild-type mice whose BM had been replaced with wild-type or *Klf5*$^{+/-}$ BM were subjected to UUO or sham operation, as shown in Figure 12**A**. Renal injury was assessed on the indicated days after UUO. No significant difference was observed between mice transplanted with wild-type BM and those transplanted with *Klf5*$^{+/-}$ BM at any time under any conditions. n=5.

Supplementary Figure 17. Myeloid-specific *Klf5* deletion

(A) Quantitative analysis of the recombination efficacy of the floxed *Klf5* alleles in bone marrow-derived macrophages (BMDMs) prepared from wild-type, *Klf5*$^{fl/fl}$, and *Klf5*$^{fl/fl}$;*LysM-Cre* mice, and from CD11b^{+}F4/80^{+} cells isolated from the kidneys of *Klf5*$^{fl/fl}$;*LysM-Cre* mice 1 day after UUO. n=6. (B) CD11b^{+}F4/80^{low} and CD11b^{+}F4/80^{hi} cell fractions among total live cells isolated from kidneys of wild-type and *Klf5*$^{fl/fl}$;*LysM-Cre* mice on the indicated days after UUO. n=3.

Supplementary Figure 18. Effects of cell type-specific *Klf5* deletion on renal injury induced by UUO

Renal pathology was assessed on the indicated days after UUO in *Klf5*$^{fl/fl}$, *Klf5*$^{fl/fl}$;*Aqp2-Cre* and *Klf5*$^{fl/fl}$;*LysM-Cre* mice. **P*<0.05 vs. *Klf5*$^{fl/fl}$ on the same day. n=3.

Supplemental Figure 19. Collecting duct-specific *Klf5* deletion

(A) Collecting duct-specific deletion of floxed alleles in *Aqp2-Cre* mice was examined using *Rosa26*-stop-*LacZ* indicator mice. β-galactosidase expression was visualized using X-gal. G, glomerulus; cCD, cortical collecting duct; mCD, inner medullary collecting ducts. Scale bars, 50 μm. (B) Assessment of DNA recombination efficacy in *Klf5*$^{fl/fl}$; *Aqp2-Cre* kidney and lung using genomic PCR. The floxed allele produced the 320 bp band, while the allele recombined by Cre produced the 250 bp band (floxed-out). (C) Quantitative analysis of the recombination efficacy of the floxed *Klf5* allele in collecting duct cells (CD) and non-CD cells. (D)

Expression of KLF5 protein analyzed in non-CD and CD cells from wild-type, *Klf5*$^{+/-}$ and *Klf5*$^{fl/fl}$;*Aqp2-Cre* mice under basal conditions. (E) Hematoxylin and eosin staining of sections of kidneys (papilla) from *Klf5*$^{fl/fl}$ and *Klf5*$^{fl/fl}$;*Aqp2-Cre* mice under basal conditions. Scale bars, 50 μm.

Supplementary Table 1. Blood biochemistry and blood pressure in wild-type and *Klf5*$^{+/-}$ mice under physiological conditions

Values are means ± S.D. n=12 mice for each group.

	WT	*Klf5*$^{+/-}$	*P*
Plasma creatinine (mg/dl)	0.22 ± 0.01	0.24 ± 0.02	NS
Blood urea nitrogen (mg/dl)	30.4 ± 1.1	29.8 ± 1.4	NS
Uric acid (mg/dl)	1.1 ± 0.2	1.4 ± 0.2	NS
Sodium (mEq/L)	147 ± 1.1	148 ± 0.8	NS
Chloride (mEq/L)	102 ± 2.1	105 ± 1.5	NS
Potassium (mEq/L)	3.8 ± 0.2	4.3 ± 0.4	NS
Blood pressure (mmHg)	104.2 ± 4.2	106.4 ± 3.4	NS

Supplementary Table 2. Blood biochemistry and survival rate of wild-type and *Klf5*$^{+/-}$ mice after UUO

Values are mean ± S.D. n=12 mice for each group.

		Wild type	*Klf5*$^{+/-}$	*P*
Plasma creatinine (mg/dl)	Pre	0.23±0.013	0.23±0.016	NS
	1Mo	0.24±0.025	0.23±0.021	NS
	3Mo	0.24±0.038	0.24±0.031	NS

		Wild type	*Klf5*$^{+/-}$	*P*
Blood urea nitrogen (mg/dl)	Pre	29.4±1.14	29.8±1.31	NS
	1Mo	30.1±1.24	29.8±1.11	NS
	3Mo	30.0±1.31	29.4±1.49	NS

		Wild type	*Klf5*$^{+/-}$	*P*
pottasium (mEq/L)	Pre	4.0±0.32	4.1±0.39	NS
	1Mo	4.0±0.29	4.0±0.30	NS
	3Mo	4.1±0.19	4.0±0.28	NS

		Wild type	*Klf5*$^{+/-}$	*P*
Uria acid (mEq/L)	Pre	1.2±0.14	1.3±0.18	NS
	1Mo	1.4±0.19	1.3±0.17	NS
	3Mo	1.4±0.20	1.4±0.19	NS

		Wild type	*Klf5*$^{+/-}$	*P*
Survival(%)	Pre	100±0	100±0	NS
	1Mo	100±0	100±0	NS
	3Mo	100±0	100±0	NS

Supplementary Table 3. Top 30 genes upregulated by Ad-*KLF5*

Unigene	Gene Title	Gene Symbol	Fold increase (Ad-*KLF5* vs, Ad-empty)
Mm.2128	S100 calcium binding protein A9 (calgranulin B)	S100a9	86.2
Mm.46425	keratin complex 2, basic, gene 4	Krt2-4	55.6
Mm.46425	keratin complex 2, basic, gene 4	Krt2-4	51.8
Mm.30138	RIKEN cDNA 1110014F24 gene	1110014F24Rik	34.1
Mm.250717	suprabasin	Sbsn	30.8
Mm.250717	suprabasin	Sbsn	28.4
Mm.36777	RIKEN cDNA 1810007E14 gene	1810007E14Rik	22.2
Mm.158766	RIKEN cDNA 2310007B03 gene	2310007B03Rik	20.5
Mm.197422	glutathione S-transferase, alpha 1 (Ya) /// glutathione S-transferase, alpha 2 (Yc2)	Gsta1 /// Gsta2	17.9
Mm.3267	annexin A8	Anxa8	17.3
Mm.4757	cellular retinoic acid binding protein II	Crabp2	16.6
Mm.3089	uroplakin 3B	Upk3b	16.0
Mm.6974	keratin complex 1, acidic, gene 14	Krt1-14	15.5
Mm.154144	arginase 1, liver	Arg1	15.1
Mm.251322	enolase 3, beta muscle	Eno3	14.6
Mm.6974	keratin complex 1, acidic, gene 14	Krt1-14	14.2
Mm.3267	annexin A8	Anxa8	13.7
Mm.25405	activity regulated cytoskeletal-associated protein	Arc	12.5
Mm.21567	S100 calcium binding protein A8 (calgranulin A)	S100a8	12.4
Mm.271868	lysosomal-associated protein transmembrane 5	Laptm5	12.3
Mm.275434	prostaglandin-endoperoxide synthase 1	Ptgs1	11.4
Mm.206774	carboxypeptidase N, polypeptide 1	Cpn1	11.2
Mm.178767	lysyl oxidase-like 4	Loxl4	11.2
Mm.265786	Heparanase	Hpse	11.1
Mm.3089	uroplakin 3B	Upk3b	10.4
Mm.250717	suprabasin	Sbsn	10.3
Mm.334344	pleckstrin homology-like domain, family A, member 2	Phlda2	10.2
Mm.272188	serine (or cysteine) peptidase inhibitor, clade B, member 6c	Serpinb6c	10.1
Mm.154087	microtubule-associated protein 6	Mtap6	10.1
Mm.35789	synaptopodin 2-like	Synpo2l	10.0

GEO sample accession number is GSE29323.

Supplementary Table 4. Blood biochemistry and blood pressure in wild-type and *Klf5$^{fl/fl}$;Aqp2-Cre* mice under physiological conditions

Values are means ± S.D. n=6 mice for each group.

	Klf5$^{fl/fl}$	*Klf5$^{fl/fl}$;Aqp2-Cre*	*P*
Plasma creatinine (mg/dl)	0.27± 0.04	0.26± 0.03	NS
Blood urea nitrogen (mg/dl)	28.2 ± 1.2	28.1 ± 1.4	NS
Sodium (mEq/L)	148.2 ± 0.9	147.8 ± 1.1	NS
Chloride (mEq/L)	116.2 ± 2.1	118.2 ± 1.6	NS
Potassium (mEq/L)	5.4 ± 0.3	5.4 ± 0.2	NS
Blood pressure (mmHg)	108.4 ± 5.1	109.6 ± 4.6	NS

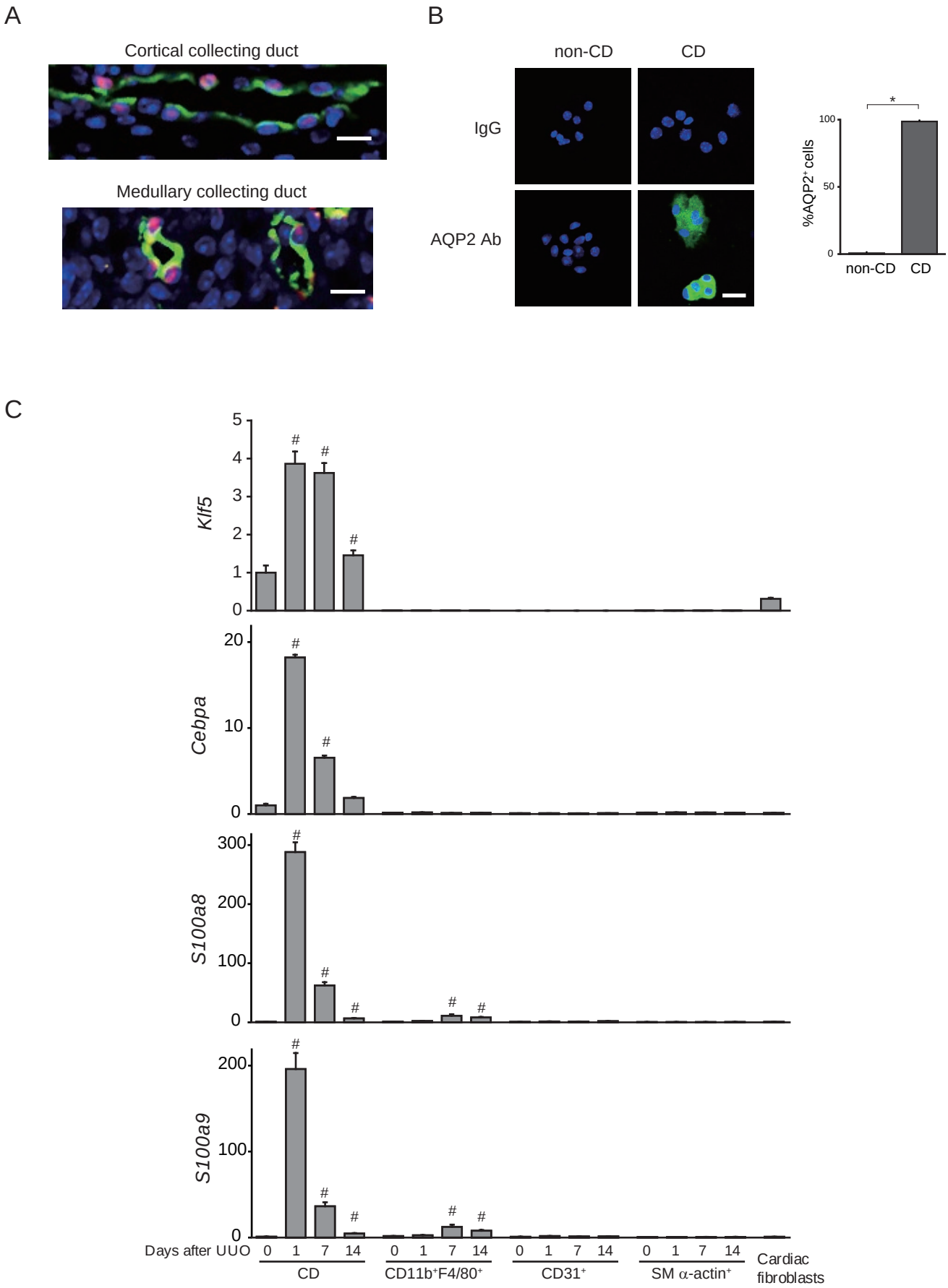

Supplementary Figure 1

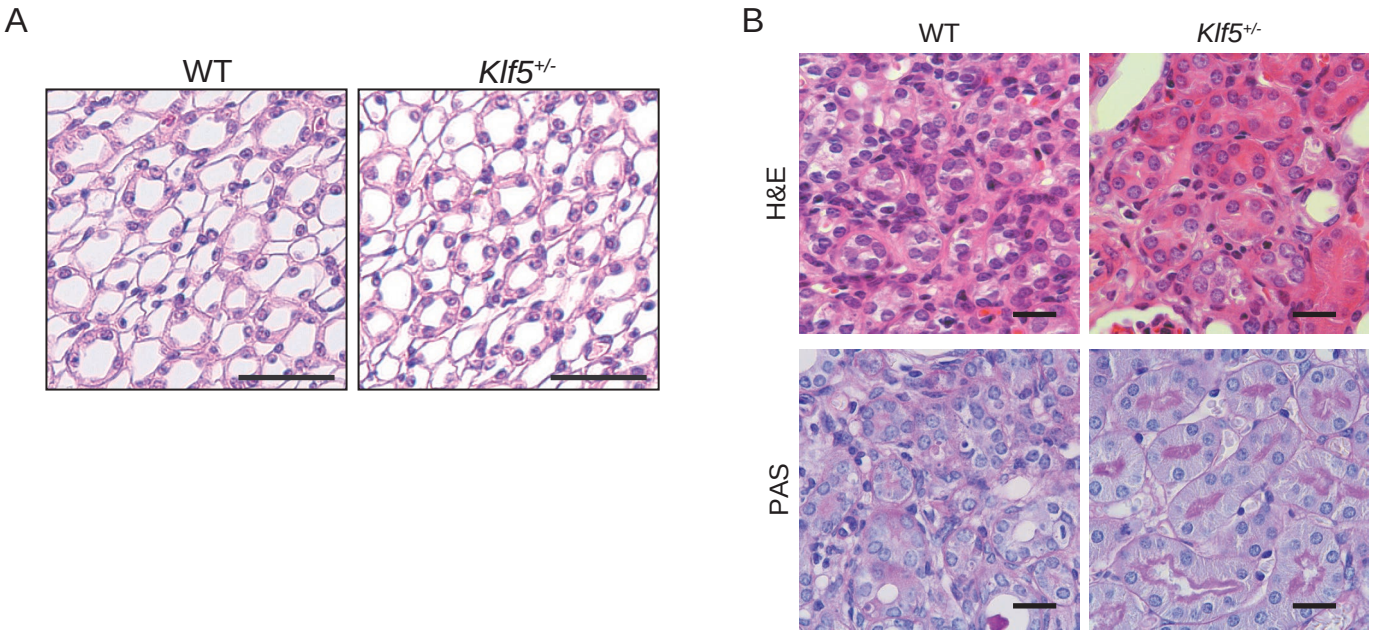

Supplementary Figure 2

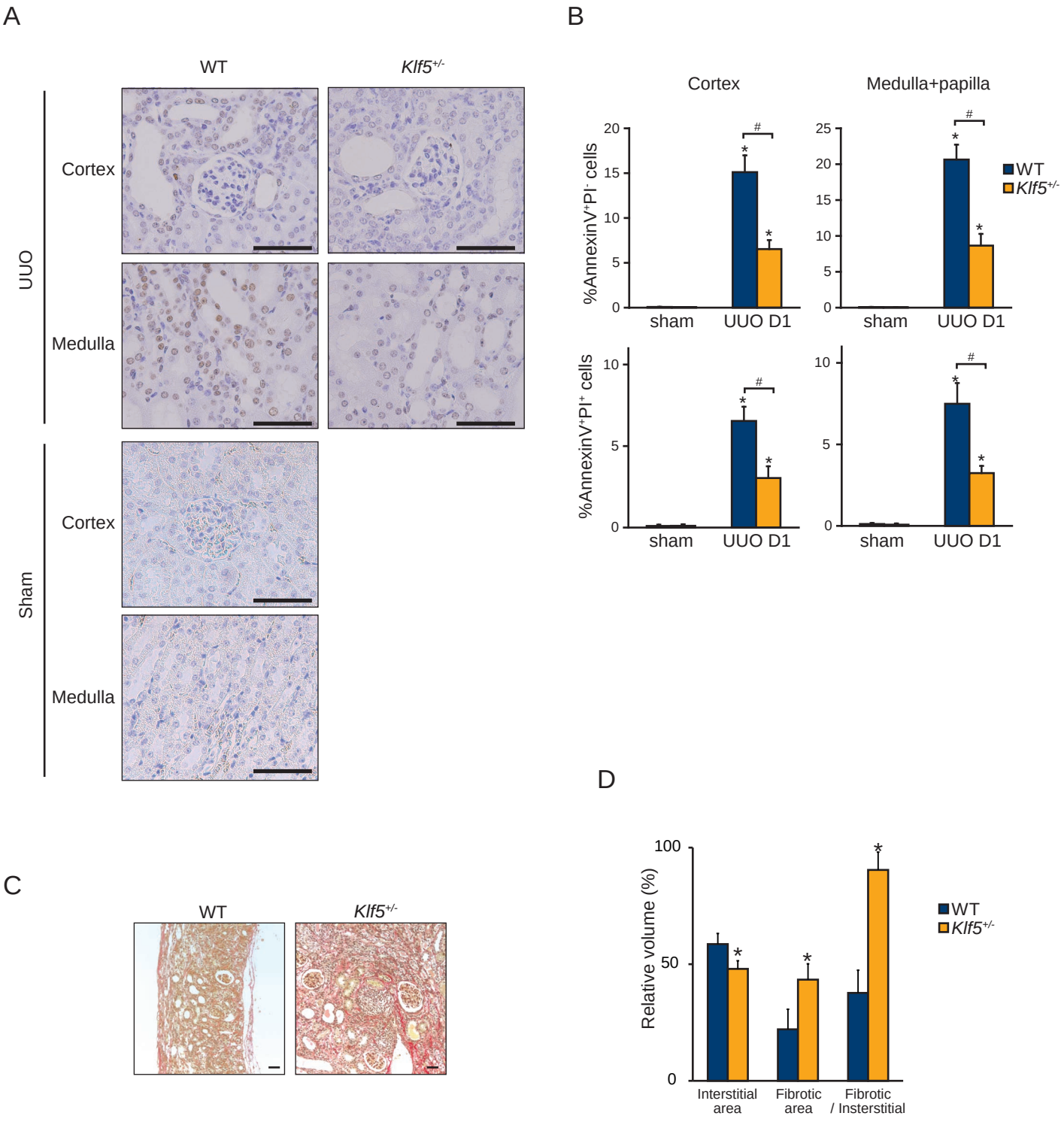

Supplementary Figure 3

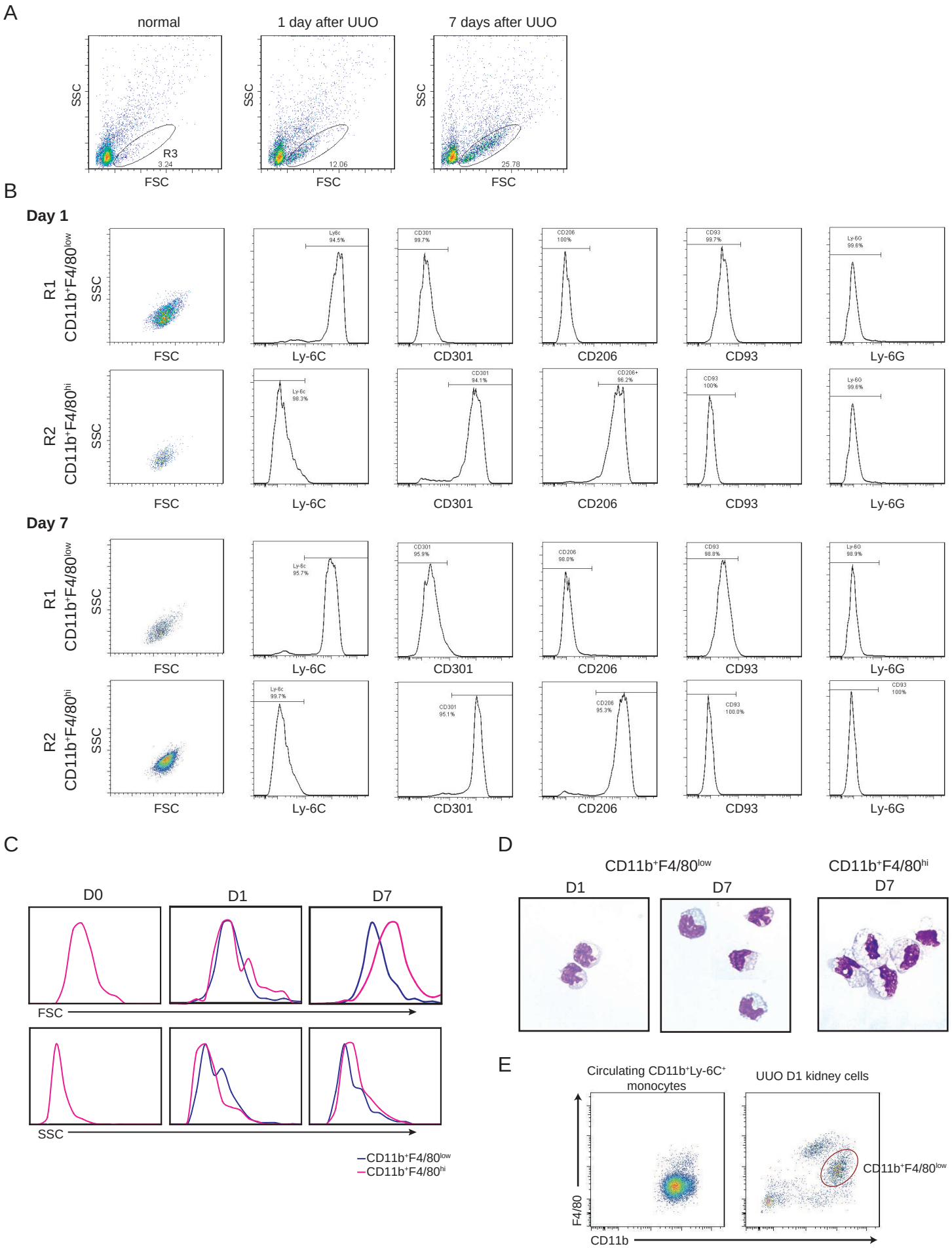

Supplementary Figure 4

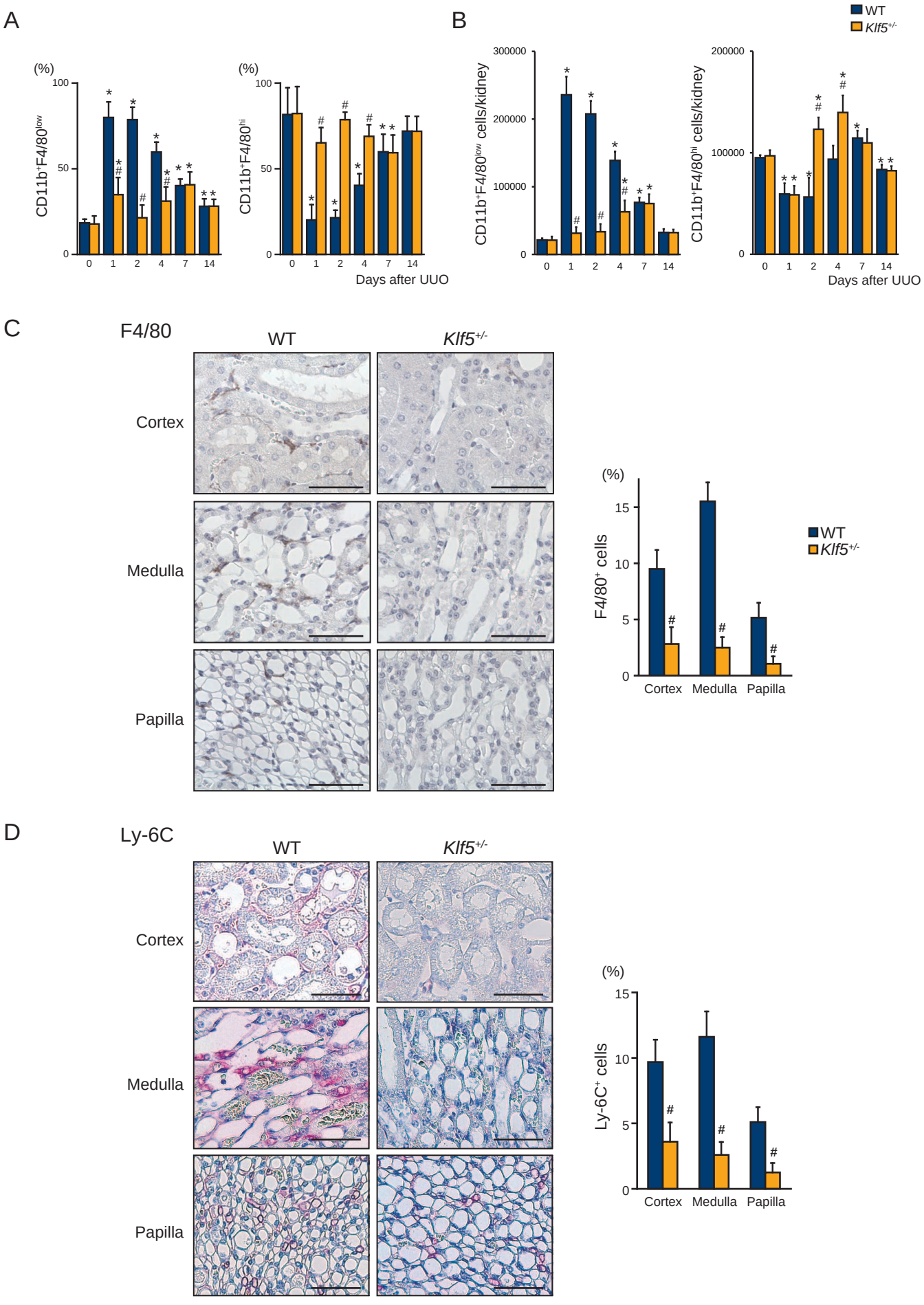

Supplementary Figure 5

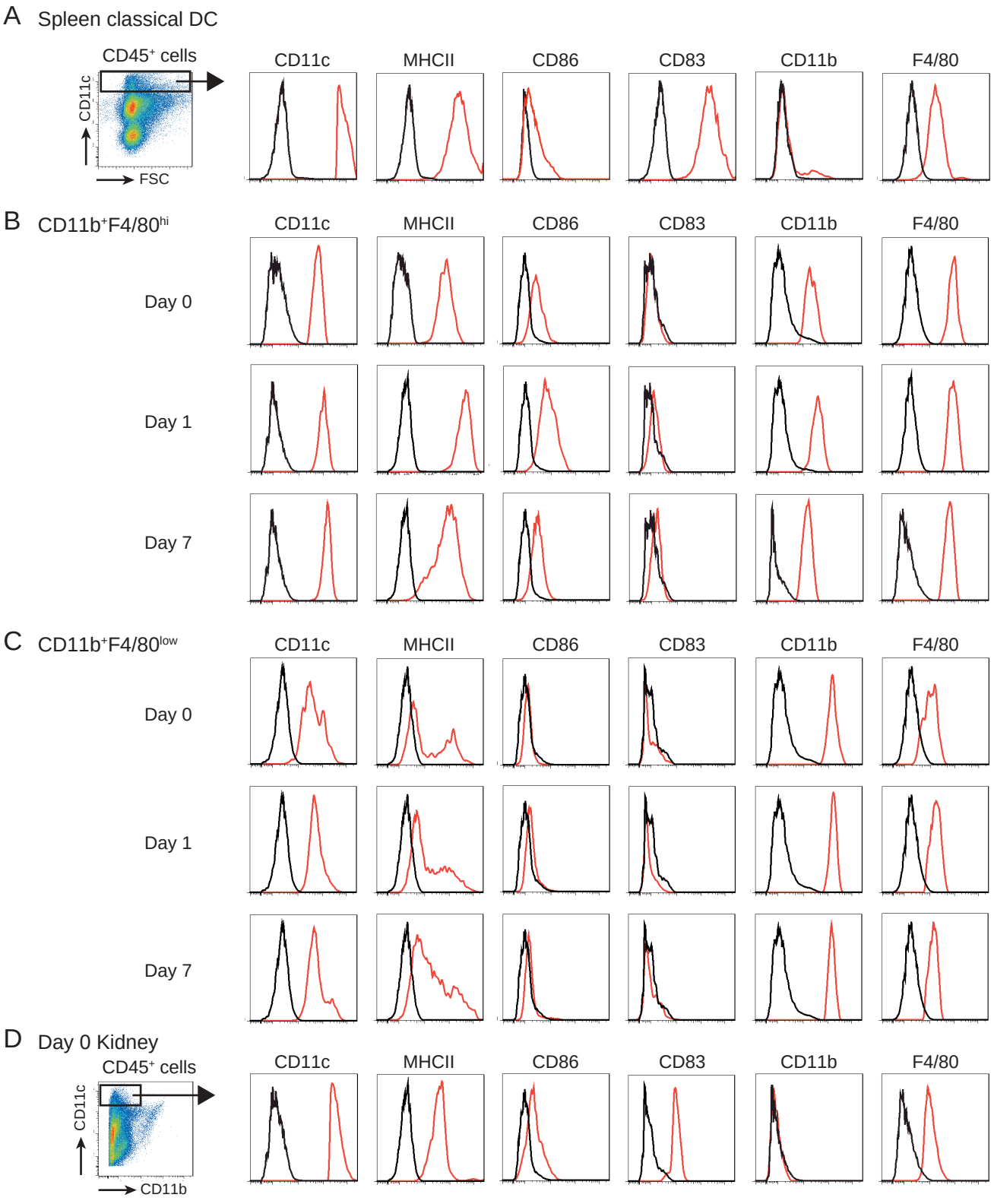

Supplementary Figure 6

A

Splenic classical DCs

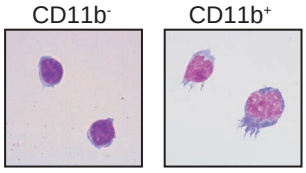

B

Kidney CD11c^{hi} cells

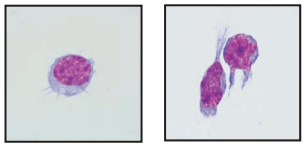

C

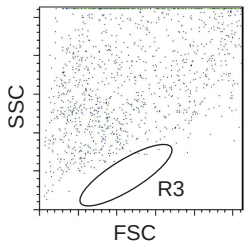

D

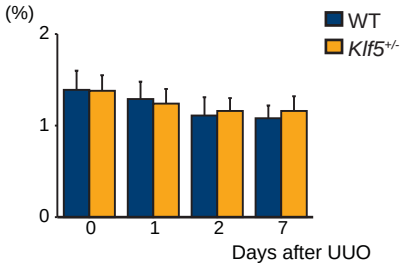

Supplementary Figure 7

A

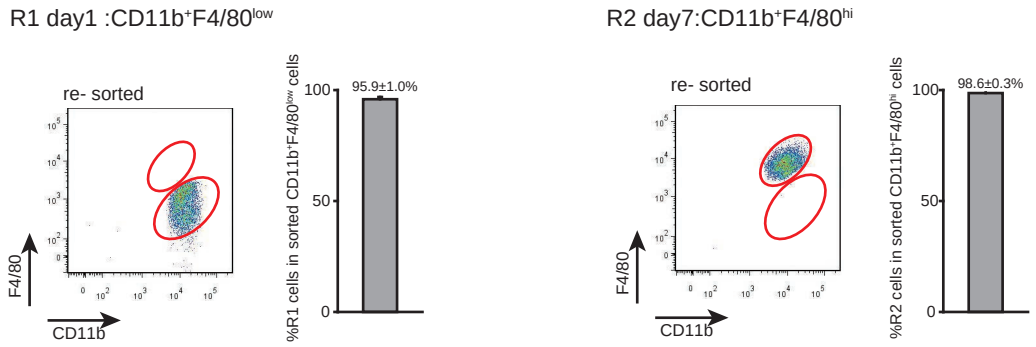

B

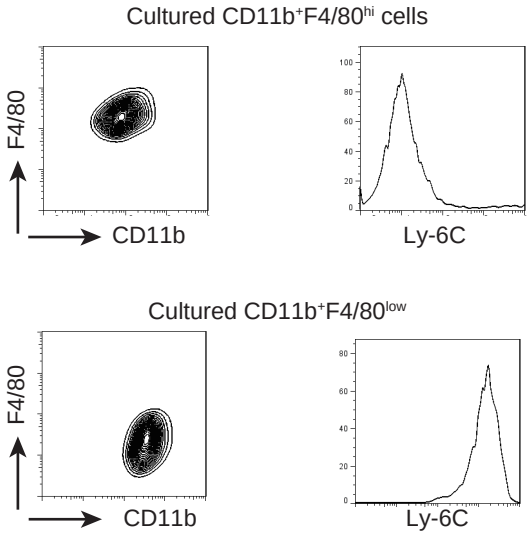

C

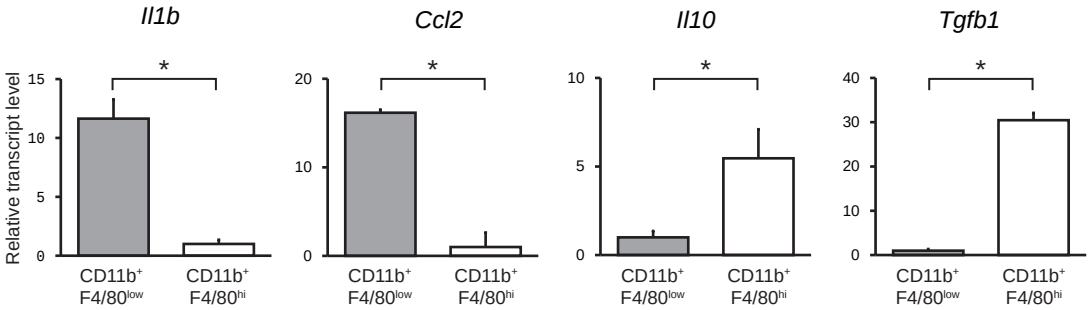

Supplementary Figure 8

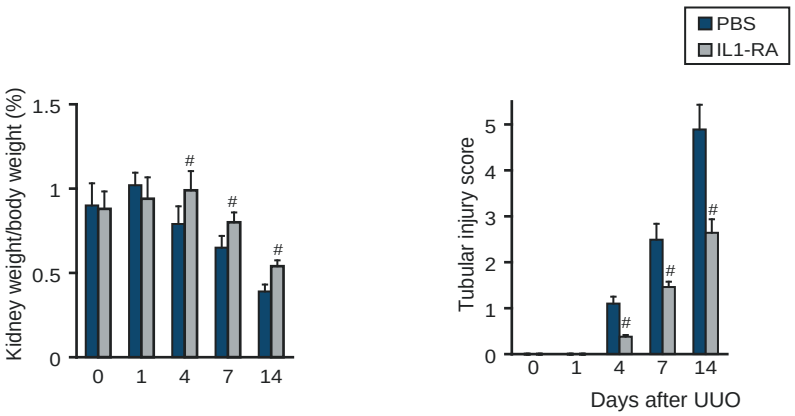

Supplementary Figure 9

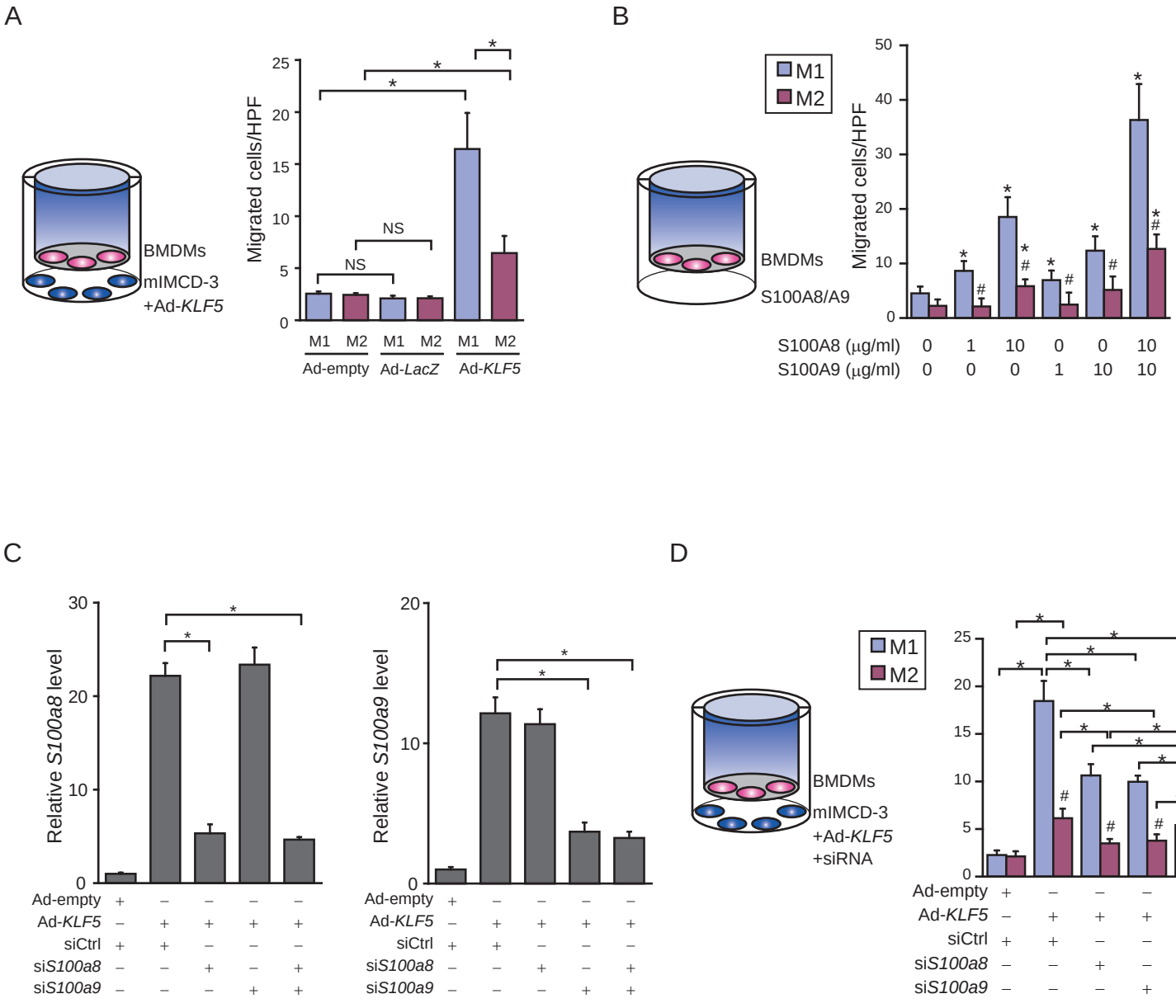

Supplementary Figure 10

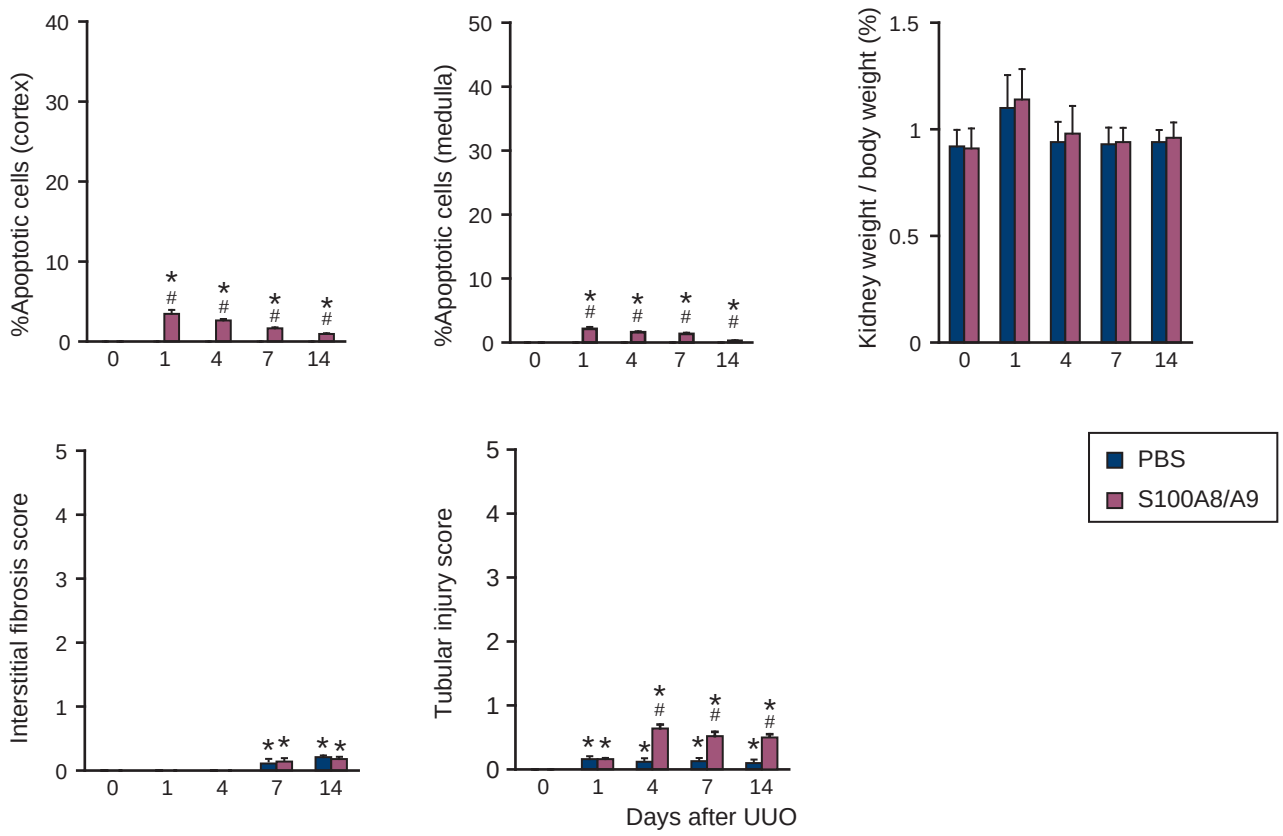

Supplementary Figure 11

A

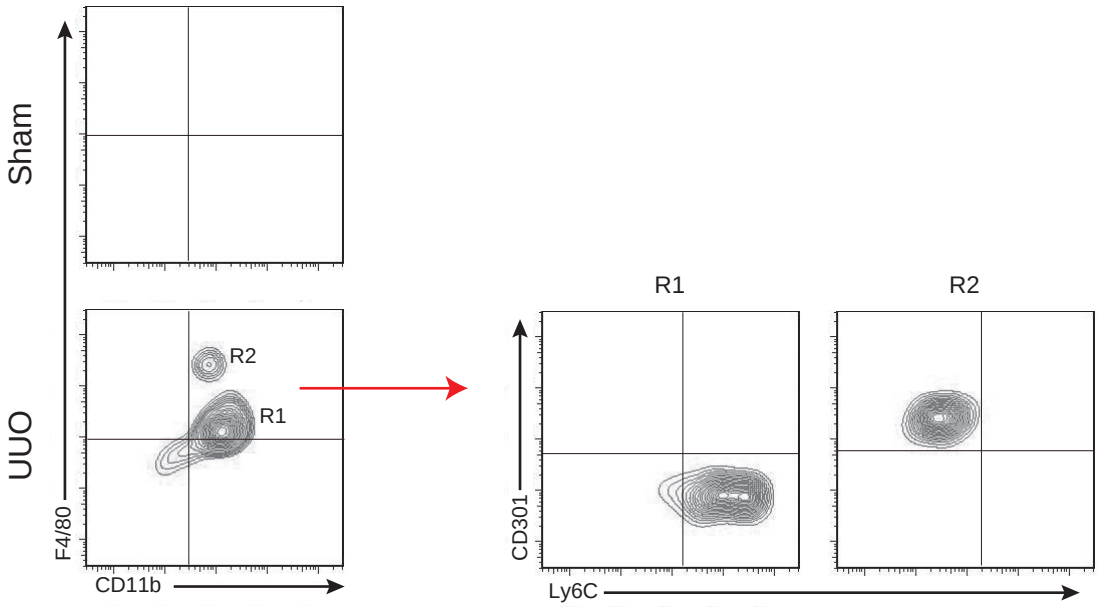

B

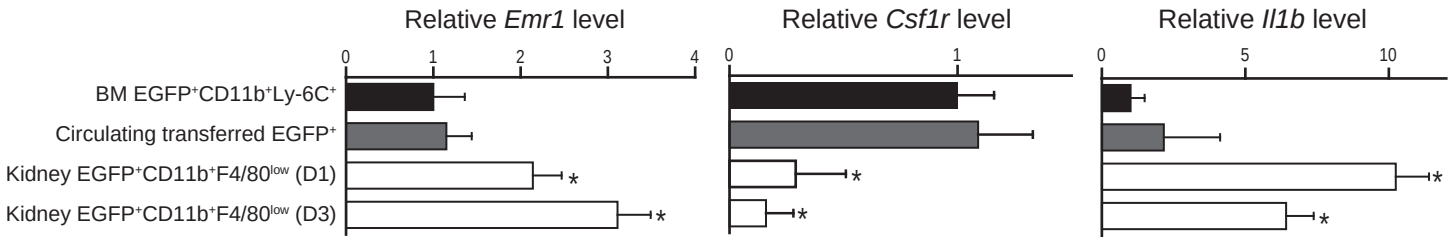

C

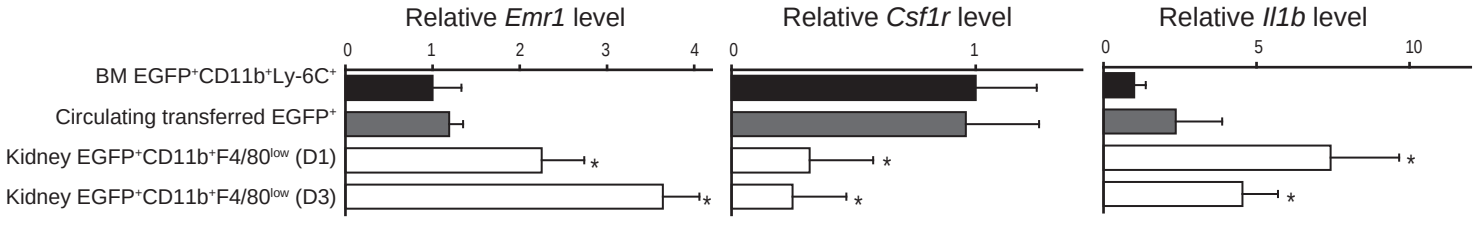

Supplementary Figure 12

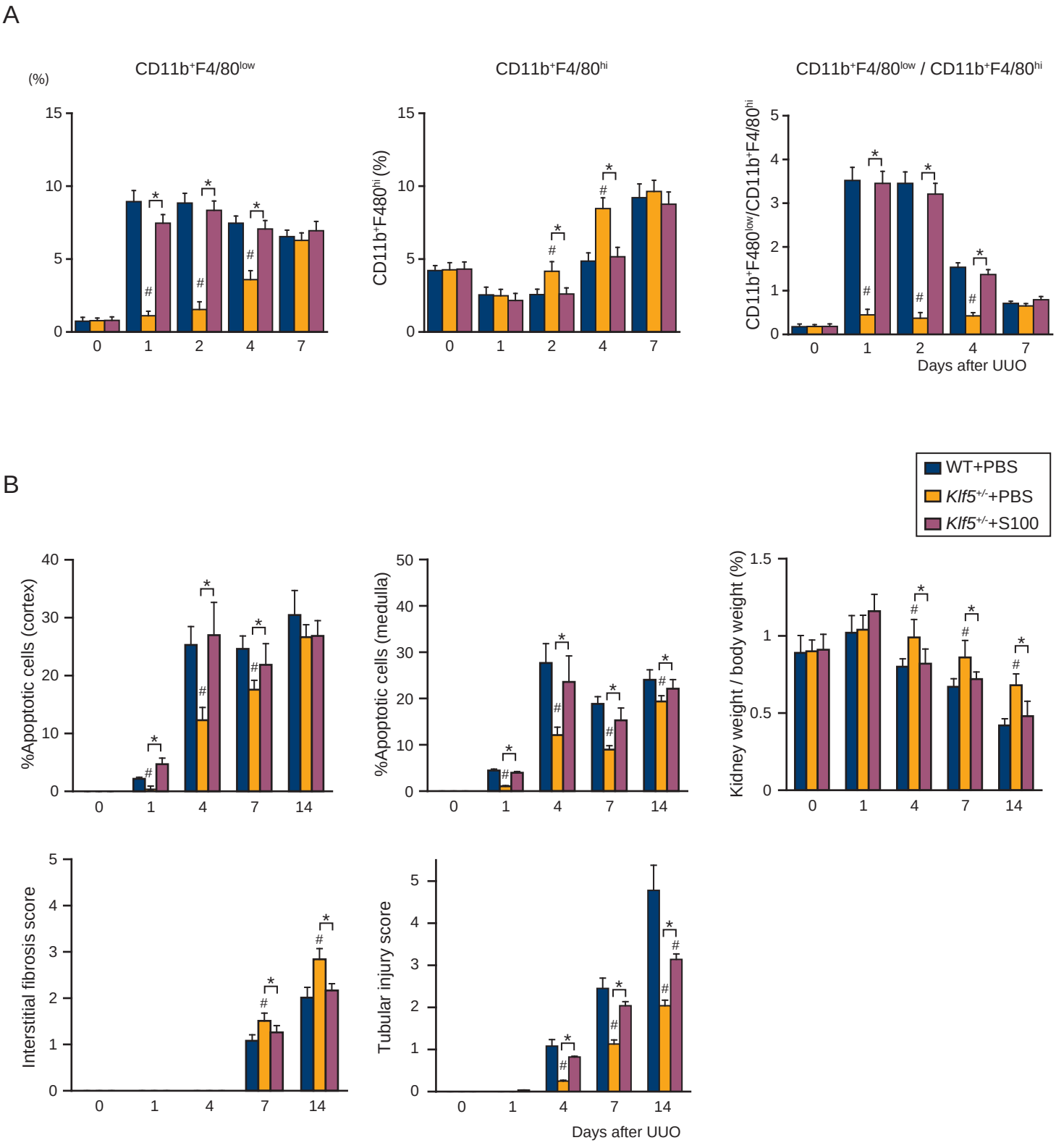

Supplementary Figure 13

A

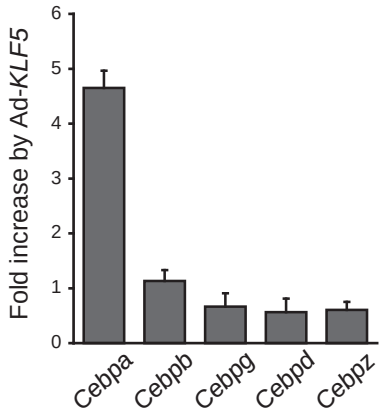

B

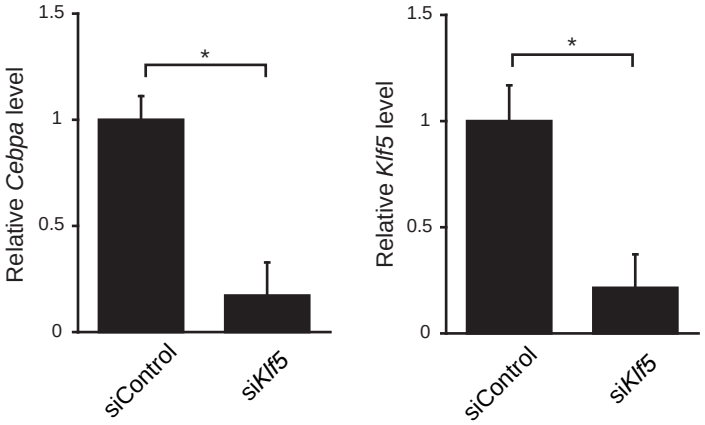

C

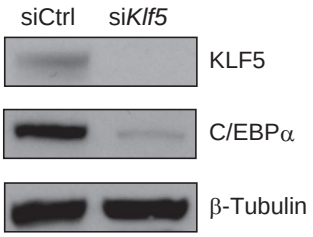

Supplementary Figure 14

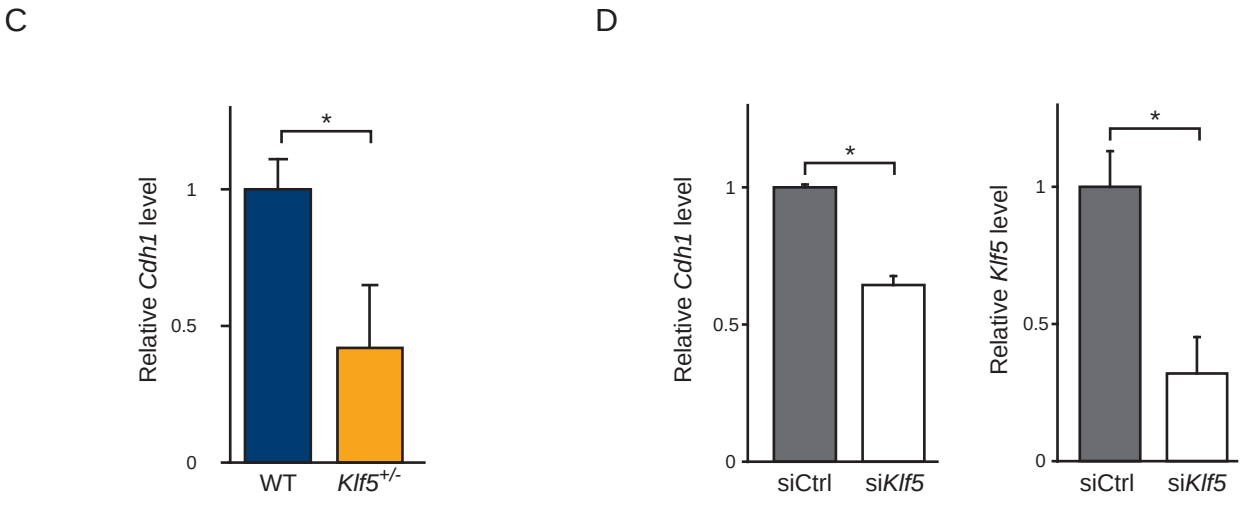

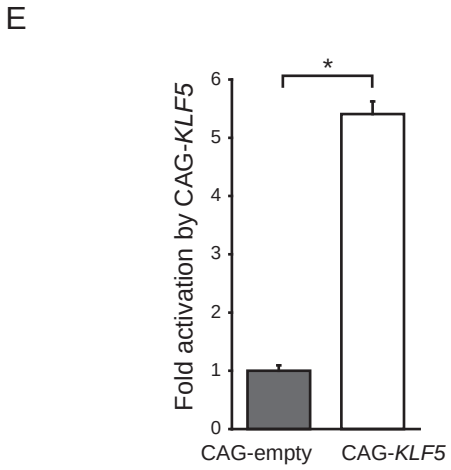

Supplementary Figure 15

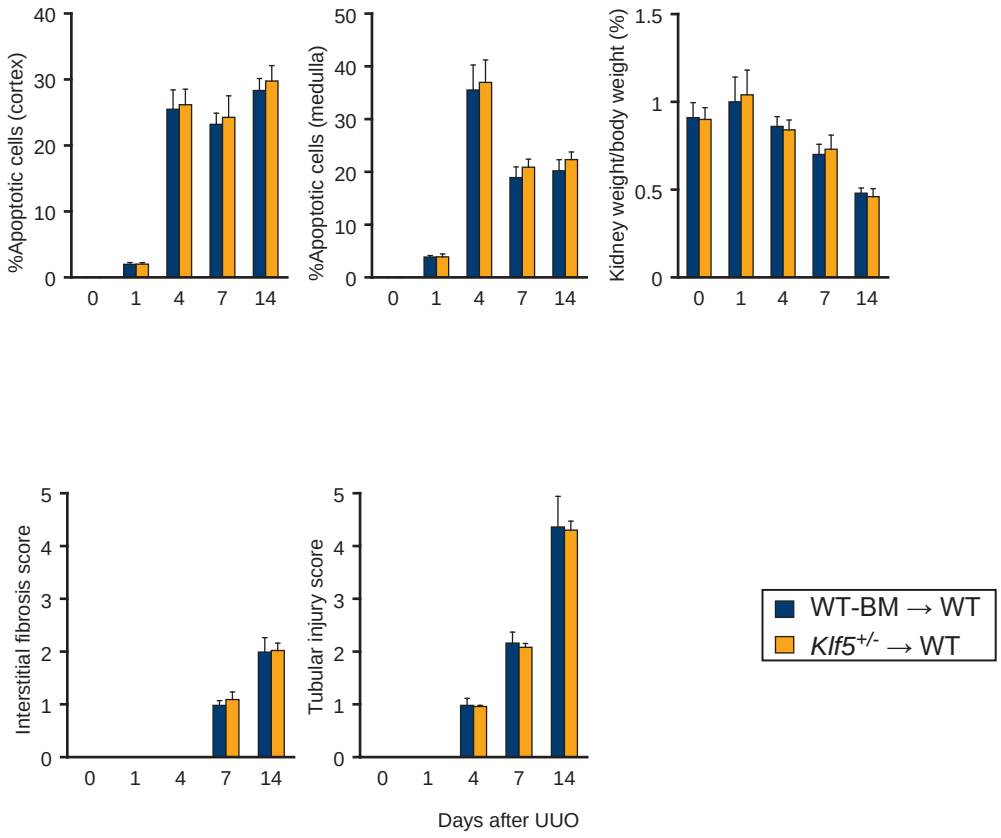

Supplementary Figure 16

A

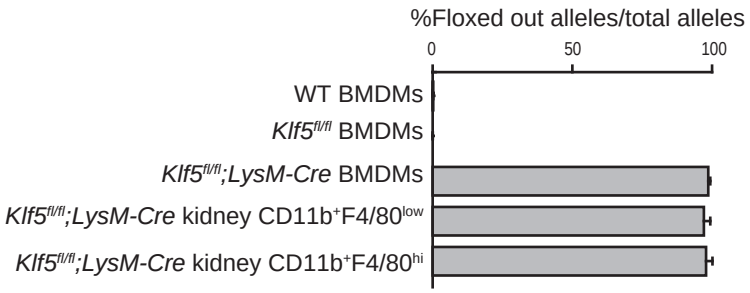

B

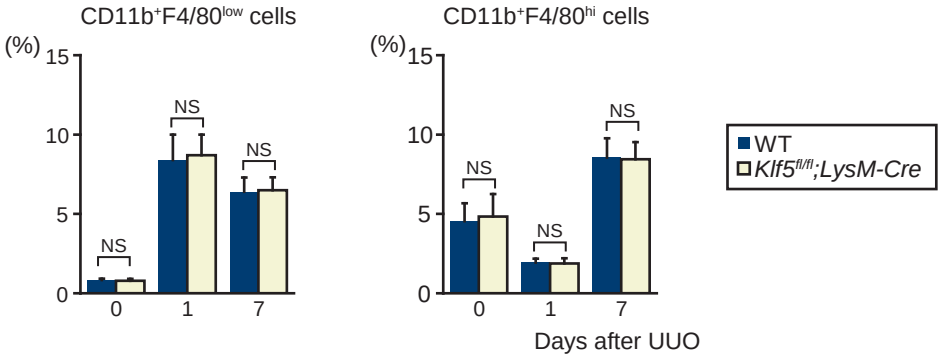

Supplementary Figure 17

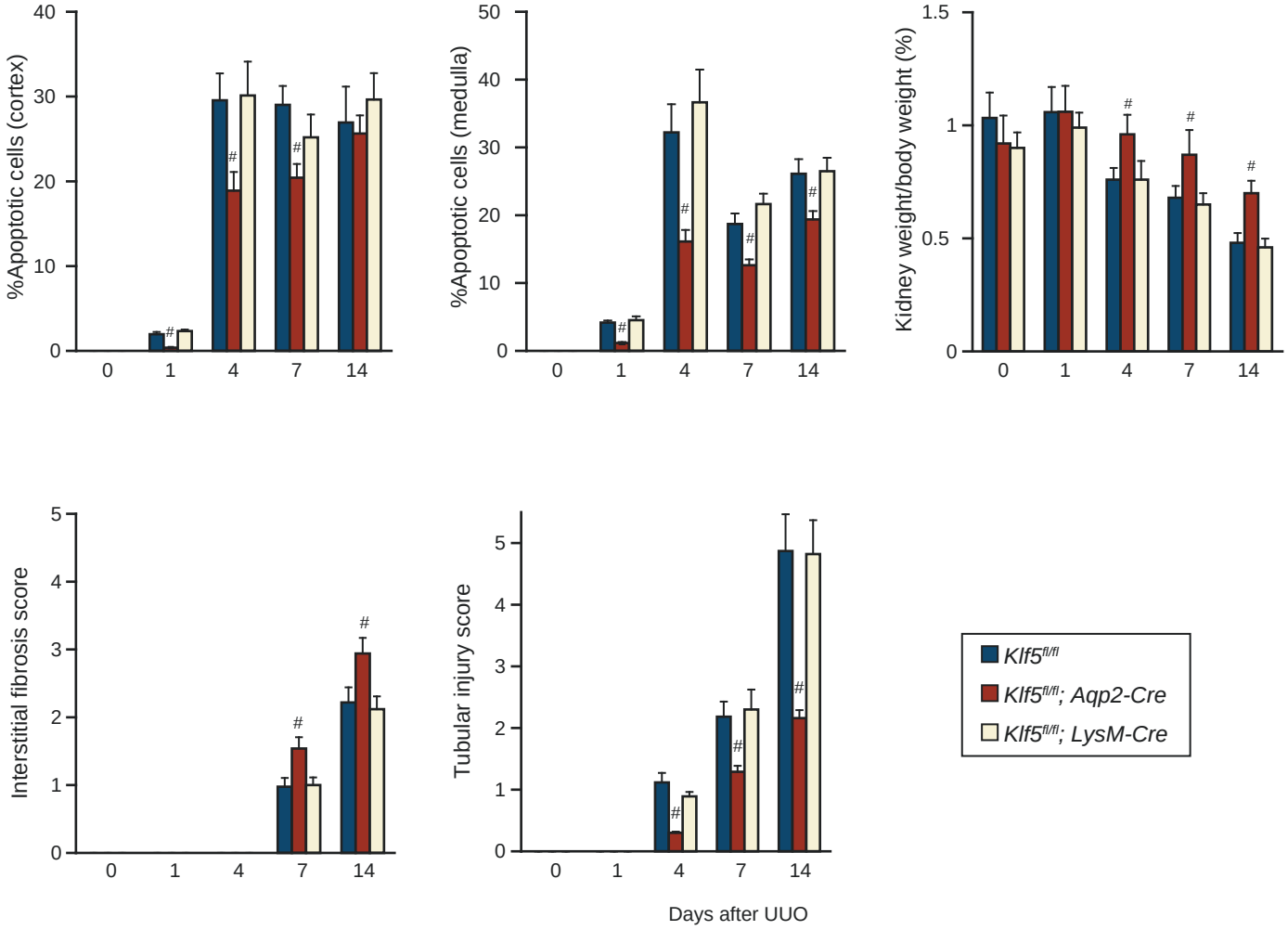

Supplementary Figure 18

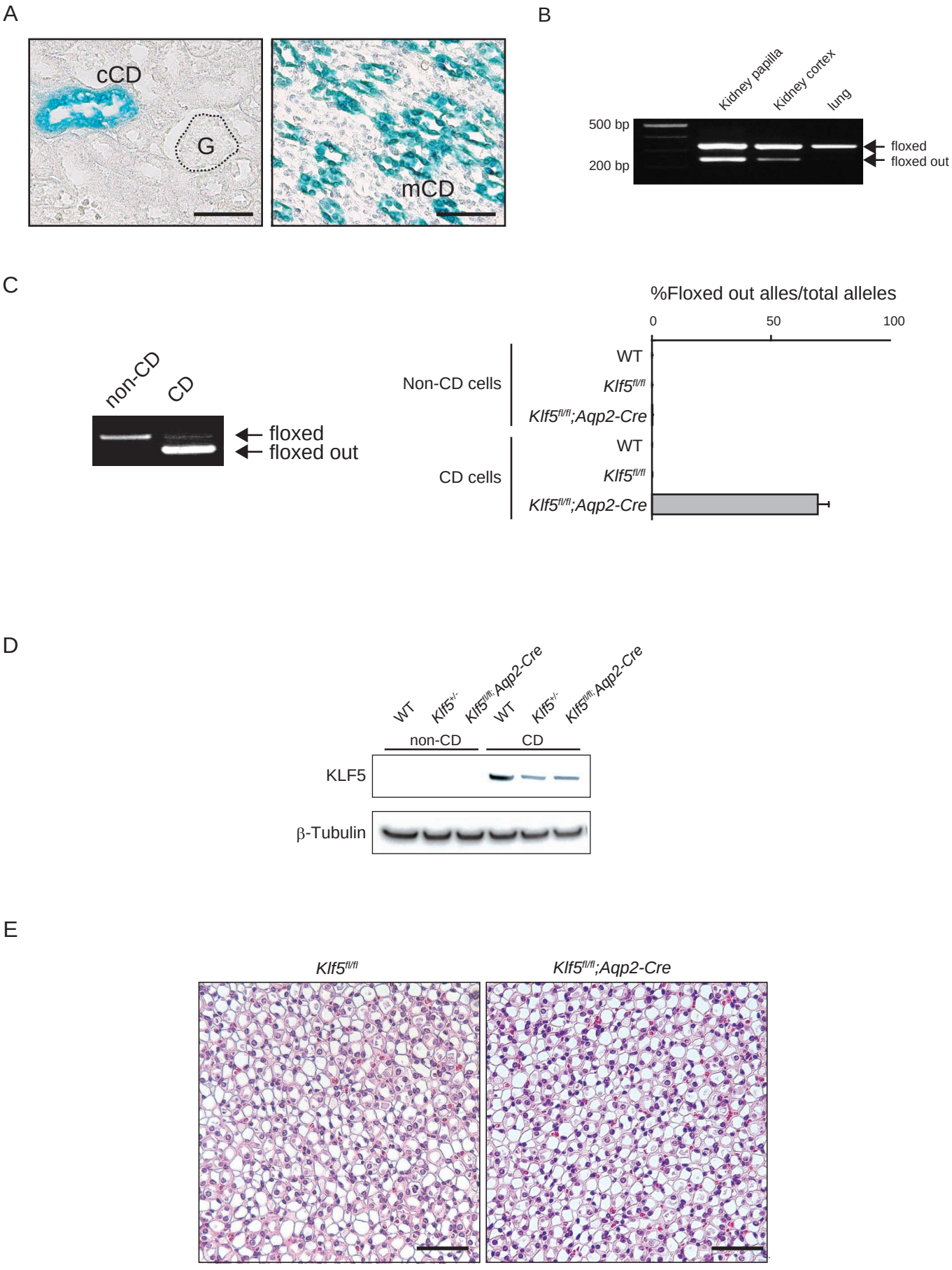

Supplementary Figure 19